Titanium Dioxide

Subjects: Others

Contributor: Danhong Wang

TiO_2 probably plays the most important role in photocatalysis due to its excellent chemical and physical properties. However, the band gap of TiO_2 corresponds to the Ultraviolet (UV) region, which is inactive under visible irradiation. At present, TiO_2 has become activated in the visible light region by metal and nonmetal doping and the fabrication of composites. Recently, nano-TiO_2 has attracted much attention due to its characteristics of larger specific surface area and more exposed surface active sites. nano-TiO_2 has been obtained in many morphologies such as ultrathin nanosheets, nanotubes, and hollow nanospheres.

Keywords: nano-TiO2 ; photocatalytic applications ; visible light ; doping ; vacancy ; composite

1. Introduction

Fossil fuel is a non-renewable resource with limited reserves [1–3]. Over the past 140 years, we have consumed one trillion barrels of oil, and today, the world's demand for energy has exceeded 1000 barrels of oil, 100,000 cubic meters of natural gas, and 221 tons of coal per second [4]. It is clear that the consumption of fossil fuels is not sustainable in the long-term and has caused serious harm to the environment and human health [5]. It is reported in [6] that the energy challenges we face are related to the "tragedy of the commons": we treat fossil fuels as resources that can be extracted and used in any way by anyone, anywhere, and use the Earth's atmosphere and oceans as landfills, emitting more than 30 Gt of CO_2 per year [7].

Dyes play an important role in various sectors of the dyeing and textile industries, most of which are synthetic dyes. These dyes usually come from coal tar and petroleum intermediates, with the annual output of more than 7×10^5 tons [8–10]. Konstantinou and Albanis [11] mentioned that industrial and textile dyes are mostly toxic organic compounds. It is estimated that nearly 17 to 20 percent of water pollution is related to the textile finishing and dyeing industries [12]. In 1974, the Ecological and Toxicological Association of the Dyestuffs Manufacturing Industry (ETAD) was established to protect consumers by working fully with the government to minimize environmental damage by addressing issues related to the toxicological impact of the products [13]. In the ETAD survey, among the 4000 test samples, the LD_{50} value of 90% of dyes was more than 2×10^{-3} mg kg^{-1}. Of all the tested dyes, diazo, direct, and alkaline dyes showed the highest toxicity [14]. In addition to the textile industry, hair dye [15], the leather industry [16], paper industry [17], photochemical batteries [18], and luminescent solar concentrator (LSC) technologies [19–21] also use a large amount of dyes.

In order to effectively control environmental pollution and solve energy problems, it is an important task for researchers to develop efficient, stable, and green solutions. Solar energy is inexhaustible and its annual radiation energy to the surface of the Earth equivalent to about 140 trillion tons of coal burning energy. It belongs to the clean renewable pollution-free energy group and is thus the most promising energy to promote the rapid development of mankind in the future [22].

In 1972, Japanese scientists Fujishima and Honda [23] were the first to demonstrate photocatalytic splitting of water on a TiO_2 electrode. Their work promotes the semiconductor photocatalysis widely used in the field of environment and energy, which opened the door of photocatalysis and has since attracted the interest of a large number of scientific researchers. In recent years, the research and development of a nano-TiO_2 (nano-TiO_2 generally refers to particles smaller than 100 nm in at least one dimension [24–26]) photocatalyst has developed rapidly and more and more achievements have been made.

For TiO_2, as the particle size decreases, its photocatalytic activity will increase to a certain extent, showing a specific size effect. Taken together, the possible size effects of nano-TiO_2 photocatalytic materials are as follows:

(1) Quantum size effect: TiO_2 is an n-type semiconductor [27]. When its particle size is less than 50 nm, it will have different properties from single crystal semiconductors, which is called the "quantum size effect" [28]. That is, when the particle size drops to a certain value, the electron energy level near the Fermi level changes from a quasi-continuous to a discrete energy level or a widening energy gap. At this time, the potential of the conduction band becomes more negative,

and the potential of the valence band becomes more positive, thereby increasing the energy of photogenerated electrons and holes, enhancing the redox capability of the semiconductor photocatalyst and improving its photocatalytic activity [29–31].

(2) Surface area effect: First, as the particle size decreases to the nanometer, the specific surface area of the photocatalyst will greatly increase as well as the number of surface atoms, so that the light absorption efficiency will be improved and the surface photocarrier concentration will increase accordingly, so the surface redox reaction efficiency is thus improved [32]. Second, as the particle size decreases, the specific surface area increases, and the bonding state and electronic state of the surface are different from the inside. The unsaturated coordination of surface atoms leads to an increase in surface active sites. Therefore, compared with powders of large particle sizes, their number of surface active sites are higher, so the adsorption capacity of the substrate is enhanced, and the reaction activity is increased [33]. In addition, the number of hydroxyl groups on the surface of the catalyst directly affects the catalytic activity during the photocatalytic reaction. When TiO_2 powder is immersed in the aqueous solution, the surface undergoes a hydroxylation process. Therefore, as the size decreases, the specific surface area increases, and the number of surface hydroxyl groups also increases, thereby improving the reaction efficiency [34,35].

(3) Carrier diffusion effect: The grain size also has a great influence on the recombination rate of photogenerated carriers. For nanoscale semiconductor particles, the particle size is usually smaller than the thickness of the space charge layer, and any effect of the space charge layer can be ignored [36]. The smaller the particle, the shorter the time for photogenerated electrons to diffuse from the crystal to the surface, and the lower the probability of electron and hole recombination in the particle will be, which improves the photocatalytic efficiency [37–39].

There have been many outstanding studies on the synthesis and modification of TiO_2 based photocatalysts and their applications in solving energy and environmental problems [40–42]. However, few articles have classified the environmental application of nano-TiO_2 and compared the specific applications of nano-TiO_2 based composites in various classifications [43–46]. By doping metal and nonmetal ions, introducing vacancy and fabricating composites with other semiconductors, the band gap of TiO_2 was adjusted to make it have better photocatalytic activity [47]. In this review, we intend to summarize the applications of nano-TiO_2 in environmental photocatalysis such as hydrogen production, carbon dioxide degradation, dye degradation, and nitrogen fixation. Finally, the current challenges and key issues of the nano-TiO_2 photocatalyst are described, which need to be addressed in future research.

2. Titanium Dioxide: An Introduction

2.1. TiO_2 Structures and Properties

In nature, TiO_2 usually has three different crystal structures: anatase, rutile, and brookite [48]. In addition, there are several metastable crystal structures of TiO_2 such as TiO_2 (H) and TiO_2II [49]. These metastable crystal structures can be obtained by artificial synthesis. Rutile is the most stable crystal form of TiO_2. Even when the particle size is reduced to the nanometer level, rutile is still the most stable TiO_2 nanomaterial. Anatase and brookite can be transformed into rutile at high temperature. Different crystal types of TiO_2 usually exhibit different morphologies and properties. Therefore, the synthesis methods and conditions for different crystal types of TiO_2 nanomaterials are also different. For example, the synthesis of anatase TiO_2 nanomaterials usually requires solution synthesis or low temperature chemical vapor deposition, however, the synthesis of rutile TiO_2 nanomaterials requires high temperature deposition or heating reaction [50].

Figure 1 is the crystal structure of three different TiO_2 phases, and the differences in crystal structures are quite evident. Rutile TiO_2 has a tetragonal structure (Figure 1b), and its {011} and {100} crystal facets have the lowest energy, therefore, its thermodynamically stable morphology is a truncated octahedron. Anatase has a tetragonal structure, and its c-axis is longer than the a-axis (Figure 1a). Anatase TiO_2 also has a low energy crystal plane, which is the same as rutile, so it can show as a truncated octahedron. The brookite belongs to an orthorhombic structure, and its structural unit is relatively larger, which is composed of eight TiO_2 units (Figure 1c).

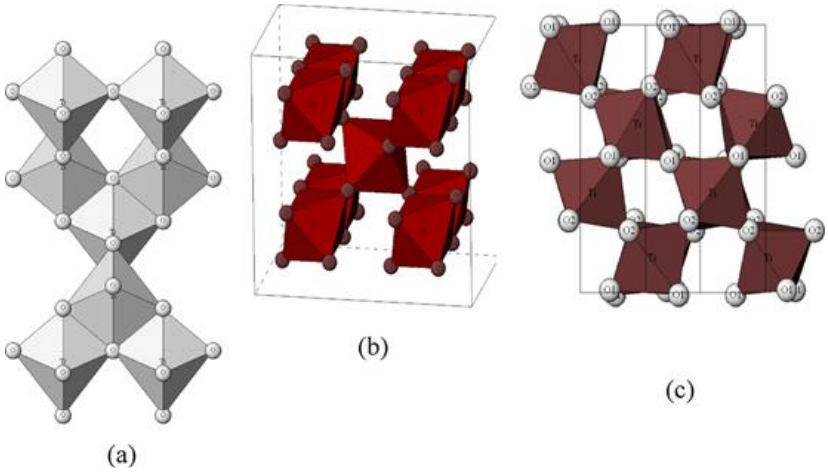

Figure 1. Crystalline structures of titanium dioxide (**a**) anatase, (**b**) rutile, and (**c**) brookite. Reprinted with permission from Advanced Industrial Science and Technology (AIST) https://staff.aist.go.jp/nomura-k/english/itscgallary-e.htm.

Jinfeng Zhang et al. [51] calculated the electronic structure and the effective mass of the carrier for anatase, rutile, and brookite TiO_2 by using the plane-wave pseudopotential method, to prove that anatase has higher photocatalytic performance than rutile and brookite. The calculation results showed that rutile had the narrowest band gap of 1.86 eV, and the band gaps of anatase and brookite were 2.13 and 2.38 eV, respectively. However, anatase is an indirect band gap semiconductor, and rutile and brookite both belong to the direct band gap semiconductor. Therefore, this leads to longer lifetimes of photogenerated electrons and holes for anatase than those for rutile and brookite. The valence bands of TiO_2 in anatase, rutile, and brookite are mainly composed of O 2p and mixed with a few Ti 3d. Above the Fermi level, the conduction band is composed of Ti 3d, mixed with a small amount of O 2p and Ti 3p. The calculation results show that the anatase has a smaller average effective mass of photogenerated electrons and holes than rutile and brookite. The smaller the effective mass of the photogenerated electrons and holes, the easier it is for them to migrate, thus improving the photocatalytic activity. As anatase has a smaller effective mass and a longer lifetime of photogenerated electrons and holes, in general, anatase TiO_2 has a higher photocatalytic activity.

The energy level structure of semiconductor material contains two aspects: energy level position and energy band width. The position of its energy level determines whether the photocatalytic reaction can take place, and the energy band width determines its light absorption range. The position of the titanium dioxide energy level is decisive for the photocatalytic reaction. From a thermodynamic point of view, when the reduction potential of the reactant is lower than the conduction band of the semiconductor material, a reduction reaction can occur; whereas when the oxidation potential is higher than the valence band of the semiconductor material, an oxidation reaction can occur [52]. Taking the photolysis of water as an example, the generation of H_2 is the process of reducing H^+ by photogenerated electrons, while the generation of O_2 molecules is the process of oxidizing O^{2-} by holes. The energy band position of TiO_2 is suitable for the photolysis of water, because the valence band of TiO_2 (+2.7 V, pH = 7) is lower than the redox potential of O_2/H_2O (+1.23 V, pH = 7) and the position of its conduction band (−0.5 V, pH = 7) is higher than the position of H_2O/H_2 redox potential (−0.41 V, pH = 7) [53].

In addition to the position of the energy level, the band width also has a very important effect on photocatalytic performance. For example, the band width (3.2 eV) of TiO_2 is wide, so it can only absorb ultraviolet light. It is only possible to use visible light when TiO_2 is doped with some metals, non-metallic elements, or combined with other semiconductors with smaller energy band widths. For example, g–C_3N_4 has a moderate forbidden band width (2.7 eV), and its conduction band position is very high (−1.3 V, pH = 7) [54]. Therefore, the combination of TiO_2 and g–C_3N_4 can improve the utilization of visible light.

2.2. Nano-TiO_2 Morphology

A large number of studies have shown that the morphology of nanomaterials has a very important effect on photocatalytic performance, because the morphology usually determines the exposure of the crystal plane and active site, specific surface area, electron, and hole transport rate and other factors.

Zero-dimensional TiO_2 nanomaterial has an isotropic structure and can expose all crystal planes (including those with higher energy), which is conducive to photocatalytic reactions. However, due to the quantum confinement effect, it has a larger forbidden band width and more surface defect states, making the photogenerated electrons and holes to have a higher recombination efficiency. If the surface can be properly modified, the recombination efficiency of electron-hole pairs

can be greatly reduced, which is conducive to improving the photocatalytic performance of zero-dimensional TiO_2 nanomaterials. This improved method has also been applied to many other zero-dimensional semiconductor nanomaterials such as carbon dots [55,56], CdS [57], CdSe [58], and graphene quantum dots [59,60].

The one-dimensional structure of TiO_2 such as nanorods, nanowires, and nanotubes possesses a very fast charge transfer rate in a single direction, and the electron-hole pair has a relatively low recombination efficiency, making it an important research object for photocatalytic reactions [61,62].

Two-dimensional TiO_2 nanosheets are very thin, with large specific surface area and effective absorption area, and the rate of charge transfer is also very fast. Therefore, two-dimensional sheet TiO_2 material is also widely used in photocatalysis [63,64].

In recent years, hierarchical structure TiO_2 nanomaterials composed of multiple morphologies have also been used in photocatalytic reactions [65,66]. These hierarchical structures of TiO_2 can simultaneously combine the advantages of different structures and effectively improve their photocatalytic performance.

Macak et al. [67] successfully prepared idealized TiO_2 nanotubes by anodizing a Ti substrate with a glycol electrolyte containing NH_4F and exploring the oxidation conditions (Figure 2a–c). The presence of hexagonal nanotubes can be clearly seen from the entire layer, arranged in neat rows, with each nanotube remaining hexagonal from top to bottom. The lower wall thickness was about 65 nm and the upper wall thickness was about 12 nm. The diameter of the internal pipe increased gradually from about 50 nm to 110 nm.

Fang et al. [68] reported a new synthesis method for TiO_2 nanometer flowers with a large amount of {001} crystal surface exposed (Figure 2d). These nanometer flowers were completely assembled from TiO_2 nanometer flakes with a size of about 2.0 μm, with a thickness of about 10–20 nm and a length of about 1.2 μm.

The submicron scale hollow sphere of TiO_2 not only has a large specific surface, but also has a size near the wavelength of UV–Vis. Therefore, in theory, diffraction and reflection caused by shell structure on the hollow sphere can improve the utilization rate of light [69]. In the presence of cationic polystyrene sphere (PS) templates, Yoshihiko Kondo et al. [70] prepared submicron hollow sphere TiO_2 by hydrolyzing isopropyl titanate (Figure 2e). Uniform anatase TiO_2 hollow pellets with a diameter of about 490 nm and a shell thickness of about 30 nm were obtained. The resulting surface area measured by Brunauer–Emmett–Teller was 70 m^2/g. The photocatalytic properties were tested by the decomposition of isopropanol under ultraviolet light.

Shuai Chen et al. [71] prepared anatase TiO_2 nanorods by electrospinning and roasting. As shown in Figure 2f, the nanorods were observed to be 200 nm to 2 μm in length and 60 nm to 150 nm in diameter. The electrical properties of TiO_2 nanobelts on curved surfaces with different curvature and their photoelectric properties under different light intensities were studied. The results showed that TiO_2 nanobelts have potential applications in flexible photodetectors and solar cells.

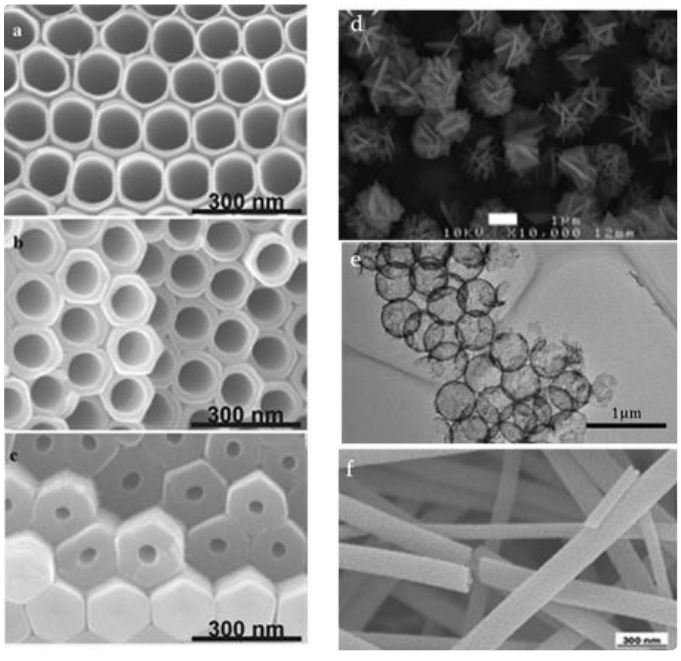

Figure 2. Scanning Electron Microscope(SEM) images of TiO_2 nanotubes taken from the upper part of the layer (**a**), the middle of the layer (**b**), and the bottom of the layer (**c**), reprinted with permission from [70]. (**d**) SEM images of flower TiO_2 reprinted with permission from [72], (e) Transmission Electron Microscope (TEM) image of TiO_2 hollow spheres reprinted with permission from [68]. (f) SEM images of TiO_2 nanobelts reprinted with permission from [70].

2.3. Strategies for Improving TiO_2 Photoactivity

Photogenic carrier recombination is a major barrier to limiting photocatalytic activity of semiconductors [71]. When recombination occurs, the excited electrons return to the valence band [73], which then do not participate in the reaction and dissipate energy in the form of radiation [74,75]. Recombination can occur on a surface as a whole, and the introduction of impurities or crystal defects can affect recombination [76]. It has been reported that doping ions [77–79], heterojunction coupling [80–82], and nanometer crystals [83,84] can promote electron-hole pair separation and reduce recombination, thus increasing photocatalytic activity.

2.3.1. Metal Doping

The absorption of visible light by wide-band gap semiconductor was originally realized by doping metal elements. According to the semiconductor band theory, due to the difference in the valence state between doped metal elements and metal elements in the semiconductor, the doped metal elements can generate donor or acceptor levels in the band gap of the semiconductor. The donor (or acceptor) energy level has two states, deep or shallow, due to the strength of the energy level binding to the electron.

As shown in Figure 3, the shallow donor level exists below the semiconductor conduction band (Figure 3a) and the shallow acceptor level exists above the semiconductor valence band (Figure 3b), while the deep donor level is close to the valence band in the semiconductor band (Figure 3c), and the deep acceptor level is close to the conduction band in the semiconductor band (Figure 3d). Electrons will jump between the donor level (or valence band) and the conduction band (or acceptor level), where the transition from the shallow donor level to the conduction band (or from the valence band to the shallow acceptor level) is a shallow transition, and the transition from the deep donor level to the conduction band (or from the valence band to the deep acceptor level) is a deep transition. Since the energy barrier to be crossed for shallow or deep transitions is smaller than the intrinsic band gap of the semiconductor, visible light can excite shallow transitions and, in most cases, deep transitions.

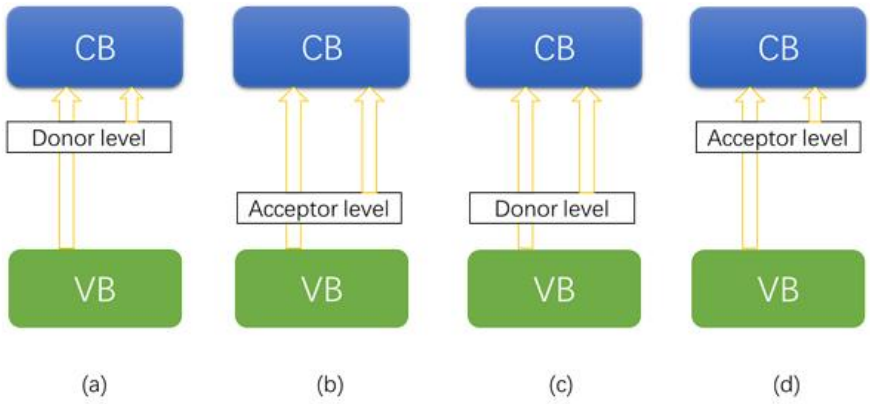

Figure 3. Effects of metal doping on band structure of semiconductors: (**a**) shallow donor level, (**b**) shallow acceptor level, (**c**) deep donor level, and (**d**) deep acceptor level formed by metal doping.

Metal doping can indeed introduce impurity levels into the wideband gap semiconductor band, and these impurity levels can also induce the absorption of visible light, but not always the improvement of photocatalytic efficiency under visible light. The current widely accepted explanation for this problem is that metal dopants may become the composite centers of photogenerated electrons and holes (especially the formed deep impurity level) in semiconductor materials, thus failing to improve (or even reduce) the visible light activity of semiconductor materials. Moreover, the visible light activity of semiconductor materials is affected by the type of doping elements, the doping method (chemical synthesis, atmospheric heat treatment, magnetron sputtering, etc.), the doping amount, the doping position (substitution or clearance), and the doping distribution (volume or surface).

2.3.2. Non-Metal Doping

Due to the bottleneck problem of metal doping, non-metal doping research has gradually become the mainstream since 2001, when Asahi et al. [85] reported the visible activity of N-doped TiO_2. In the past decade, important progress has been made in studies on non-metal doping including synthesis, characterization, mechanism research, and performance.

According to the band theory of semiconductors, the energy band of the semiconductor is a new molecular orbital formed by the hybridization of atomic orbitals of constituent atoms. The conduction band and valence band of most transition metal oxides (including TiO_2) are mainly composed of 3d metal orbital and 2p oxygen orbital, respectively. Again, on the basis of molecular orbital theory, when some of the oxygen atoms in the lattice of TiO_2 are replaced with an element that is less electronegative than oxygen, the electron orbitals of the doping elements with the 2p orbital of oxygen forms a new molecular orbital with lower energy than the 2p orbital of oxygen, that is, the top of valence band formed by this new molecular orbital is higher than the top of the valence band formed by the 2p orbital of oxygen. However, the 3d orbit of the titanium forming the conduction band does not change, so it can be seen that through the doping of elements with lower electronegativity than oxygen, the bottom of the conduction band for titanium dioxide remains unchanged, and the top of the valence band is increased, thus reducing the band gap of TiO_2. In fact, most non-metallic elements are less electronegative than oxygen, which can be used to reduce the band gap of TiO_2 through doping. In addition, a suitable dopant element, in addition to the requirement of electronegativity, should have an ion radius similar to that of oxygen ions in order to achieve atomic substitution doping.

2.3.3. Vacancy

Heteroatomic doping of semiconductors also typically introduces vacancies in the lattice. Vacancy is one of the defects of intrinsic characteristics in semiconductor materials such as oxygen vacancy in oxides and nitrogen vacancy in nitrides. Vacancy can introduce a defect level into the band gap of the semiconductor (for example, the defect level of the oxygen vacancy is located below the conduction band), thus causing visible light absorption of the semiconductor material. There are many studies on vacancy (especially oxygen vacancy [86,87]), and in most cases, the presence of vacancy can improve the catalytic activity of semiconductor materials. For example, the introduction of nitrogen vacancy in g–C_3N_4 can effectively improve the photodissociation performance of aquatic hydrogen [88]. In addition, the presence of defect levels can even enable the insulator SiO_2 (band gap > 8 eV) to have the capability of photocatalytic hydrogen production [89].

2.3.4. Composites

Photoelectron and hole in semiconductor materials are mostly recombined in the process of bulk phase diffusion or transferred to the surface, and only a few electrons and holes participate in redox reaction, which is the most fundamental factor that limits the photocatalytic activity of semiconductor materials. For a single material, a defect on its surface (such as a vacancy, etc.) will become the trapping pit of an electron or hole, thus causing the separation of photogenerated electrons and holes, but the separation is finite. To obtain more separated electrons and holes, researchers have used carrier transfers between composite semiconductors over the past few decades.

Figure 4a shows the carrier transfer in the semiconductor sensitization process, which mainly expands the light absorption range of composite semiconductor materials. Generally, the semiconductor with narrow band gap and high conduction band is combined with a semiconductor with a wide band gap and low conduction band (such as TiO_2, ZnO, etc.). In this kind of composite semiconductor material, the electrons, which can be excited by visible light to the conduction band of the narrow band gap semiconductor, are transferred to the conduction band of a wideband gap semiconductor under the drive of energy level difference.

If two semiconductor materials with staggered energy levels are combined to form a type II semiconductor heterostructure, the carrier transfer between them is shown in Figure 4b. Electrons transfer from a semiconductor with a high conduction band to a semiconductor with a low conduction band under the action of energy level difference, while holes transfer from a semiconductor with a low valence band to a semiconductor with a high valence band, thus facilitating the spatial separation of photogenerated electrons and holes. So far, most semiconductor materials can find another semiconductor material matching its energy level, and form this type II semiconductor heterostructure, and type II energy level arrangement is also the most commonly used in semiconductor combination of the semiconductor heterostructure. For example, ZnS/ZnO [90], SnO_2/ZnO [91], TiO_2/WO_3 [92], g–C_3N_4/WO_3 [93], etc.

If the semiconductor materials that make up the type II semiconductor heterostructure are p-type and n-type, respectively, and their band edges are arranged as shown in Figure 4c, then the built-in electric field in the p-n junction will further increase the carrier transfer to promote greater separation of photogenerated carriers on semiconductors. Such semiconductor heterostructures are p-In_2O_3/n-ZnO [94], p-$CaFe_2O_4$/n-ZnO [95], p-NiO/n-ZnO [96], and p-ZnO/n-TiO_2 [97], etc.

The above-mentioned type II semiconductor heterostructure can promote the separation of photogenerated carriers of semiconductors, but there are also unfavorable factors, that is, the carriers are all transferred to the low energy level, thereby the reduction and oxidation capacity of photogenerated electrons and holes is reduced. If the separation of photogenerated carriers can be achieved while maintaining their ability for oxidation and reduction, it will be beneficial for

the application of semiconductor heterostructures in photocatalysis. For this, the research in some specific II type semiconductor heterostructures (for example, the CdS/ZnO [98], $WO_3/CaFe_2O_4$ [99], CdS/WO_3 [100], BiOI/g–C_3N_4 [101], etc.) puts forward the concept of the mechanism of the vector Z carrier transfer (Figure 4d). Taking CdS/ZnO as an example, during the carrier transfer process of the vectorial Z-scheme mechanism, the photogenerated electrons on ZnO and the photogenerated holes on CdS recombine at the interface, thus, the photogenerated electrons on CdS with stronger reducibility and the photo-generated holes on ZnO with stronger oxidability are retained.

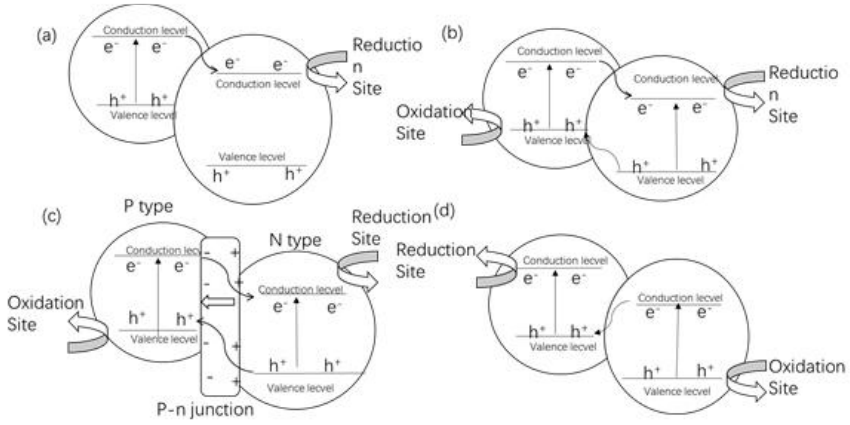

Figure 4. Charge-carrier transfer process in sensitization (**a**), traditional (**b**), p-n junction (**c**), and vectorial Z-scheme (**d**) mechanisms.

3. Photocatalytic Hydrogen Production

Hydrogen (H_2), with its heat of combustion, is expected to be an important energy source on the world energy stage. So far, a number of methods have been implemented to obtain hydrogen such as chemical, physical, or electrocatalytic hydrogen production [102–104]. In these methods, photocatalytic hydrogen production [105,106] has developed rapidly because it is clean, cheap, and environmentally friendly. Many materials with excellent photocatalytic hydrogen production properties have been reported such as ZnO [107], MoS_2 [108], etc. In particular, TiO_2 [109,110], which has physical and chemical stability, a unique energy band structure and photochemical activity, was first reported in 1972 [23], and has since been a research hot spot.

The principle of photocatalytic hydrogen production is shown in Figure 5 [111,112]. Photocatalysis has four main processes in Figure 5, namely, light collection (stage 1), the electron excites from the valence band to the conduction band (stage 2), photogenerated electrons and holes separation and transfer (stages 3 and 4), and surface redox reactions (stages 5 and 6) [54]. First, the energy required for photocatalysis needs to be above or equal to the band gap of the semiconductor. Generally, the semiconductor consists of the valence band and the conduction band, which are separated from each other by the forbidden band [113]. Under the appropriate conditions, the photocatalyst excites to produce electron and hole pairs ($e^- + h^+$) (Equation (1)), the electrons are excited from the valence band to the conduction band, leaving holes in the valence band. The recombination of photoelectrons and photoholes also occurs as Equation (2). Photogenerated electrons and holes participate in the redox reactions in water. The oxidation reaction is that the water reacts with h^+ to produce O_2, as shown in Equation (3), while Equation (4) shows the reduction reaction is that H^+ gains e^+ to produce H_2. When reduction and oxidation occur, the redox reaction potentials on the photocatalyst surface are higher than the conduction band and lower than the valence band levels [54,114,115]. Photogenerated holes have strong oxidation ability to oxidize water and organics (such as alcohols), as shown in Equations (3) and (5). The thermal dissociation of water can be carried out at a temperature higher than 2070 K, but the photocatalyst can be used under the light radiation to decompose water at room temperature with an energy greater than the band gap energy [116]. The mechanism of photocatalytic dye degradation [117], carbon dioxide reduction [118], and nitrogen fixation [119] is similar to the mechanism of photocatalytic hydrogen production, except that the redox potential of the reaction is different, and is not repeated below.

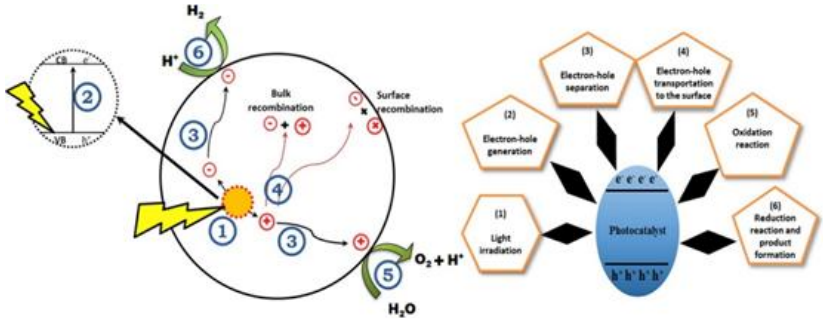

Figure 5. Photocatalytic hydrogen production mechanism. Reprinted with permission from [111].

Catalyst → Catalyst ($e^- + h^+$)	(1)
Catalyst ($e^- + h^+$) → Catalyst	(2)
$H_2O + h^+ \rightarrow O_2 + 2H^+$	(3)
$2e^- + 2H^+ \rightarrow H_2$	(4)
$RCH_2OH + 2h^+ \rightarrow RCHO + 2H^+$	(5)

The photocatalytic ability of rutile TiO_2 is in principle superior to anatase [120]. First, rutile is thermodynamically stable, while anatase is metastable [121,122]. Second, rutile exhibits more effective charge separation due to fewer defects in its crystal, because the defect is the recombination center of the photogenerated electron-hole pair [123]. Most importantly, rutile titanium dioxide has a smaller band gap (3.02 eV) than anatase (3.20 eV) [124–126]. Therefore, in theory, rutile TiO_2 has greater potential as a photocatalyst. However, due to the high photogenerated electrons and holes recombination rate of rutile TiO_2, it usually shows a lower photocatalytic performance than anatase TiO_2 [127–129]. Inspired by the concept of "surface heterojunction" [130], Chaomin Gao et al. [131] introduced the facet heterojunction (FH) strategy to promote the separation of photogenerated electrons and holes in rutile TiO_2 by building 3D layered nanostructures to obtain higher photocatalytic activity. A 3D rutile TiO_2 photocatalyst was prepared on the surface of TiO_2 nanorods (NRs) coated with ultrathin TiO_2 nanocrystalline sheets. This 3D rutile TiO_2 contained countless FH, which are formed by nanosheets with different levels on the interface between the coated nanosheets and the nanorod substrate. In order to clarify its high activity, FH-TiO_2 was compared with rutile TiO_2, anatase TiO_2, and P25, and the yield of H_2 production for FH-TiO_2 was 1.441 mmol g^{-1} h^{-1}, which was much higher than the other photocatalysts (Figure 6).

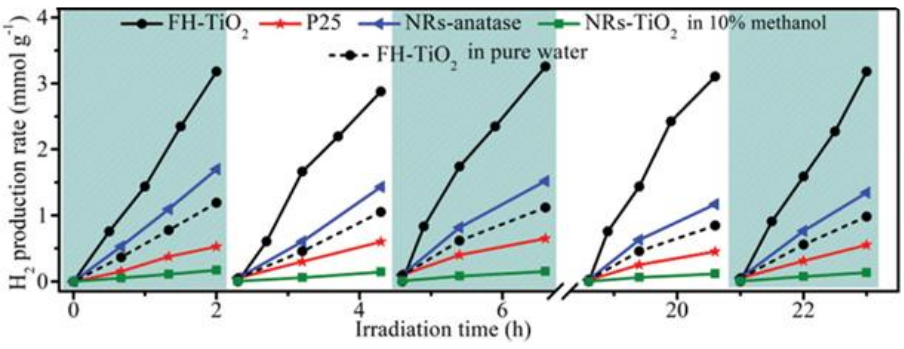

Figure 6. Photocatalytic hydrogen production cycle experiment. One wt% Pt as a cocatalyst was loaded on FH-TiO_2, P25, NRs-anatase, and NRs-TiO_2. Reprinted with permission from [131].

A large number of mesoporous TiO_2 materials with interpenetrating and regular mesoporous systems have been studied in a large body of research [132–134]. They have great potential in photocatalysis [135,136]. At present, many efforts have been made to pursue high-performance mesoporous TiO_2 (OMT) materials, but the results have not been good [137–140]. Wei Zhou et al. [141] (Figure 7) synthesized mesoporous black TiO_2 (OMBT) with regular pore sizes and large specific surface area (124 m^2 g^{-1}). OMBT materials can extend the optical response to visible and even infrared regions. The photocatalytic hydrogen production activity of OMBT was very high (136.2 μmol h^{-1}), and there was no significant inactivation after multiple cycles. The band gap of OMBT was significantly smaller than that of OMT, making it more susceptible to visible light excitation.

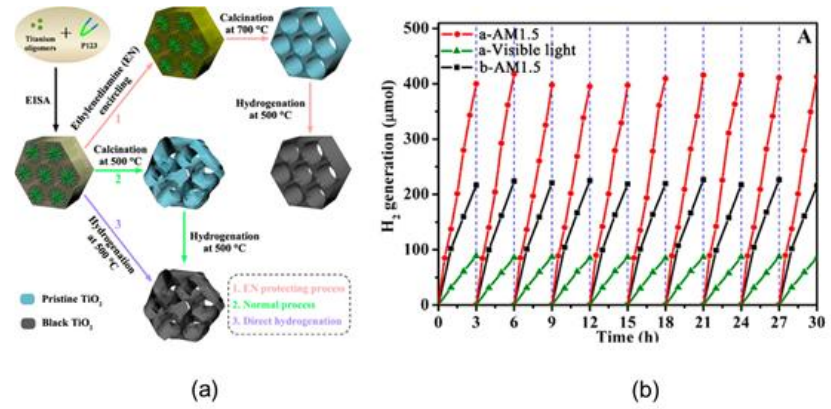

Figure 7. (**a**) The synthesis process of mesoporous black TiO_2(OMBT). (**b**) Photocatalytic hydrogen production cycle experiment under AM 1.5 and visible light irradiation. Reprinted with permission from [141].

The exposed surface of anatase TiO_2 also determines the photocatalytic capacity of water to a large extent. In order to obtain higher photocatalytic activity, shape control strategy has always been a hot research topic [102,142]. In recent years, it has been theoretically revealed that the {001} and {101} faces can effectively separate electrons and holes, so the photocatalytic activity can be improved [143]. The {101} face (0.44 J m^{-2}) has a lower surface energy than the {001} face (0.90 J m^{-2}), so the {101} face is more thermodynamic stable [144]. Various reaction systems have been developed to control the growth of anatase TiO_2 to increase the percentage of {001} face [145]. Ming Li et al. [146] (Figure 8) used ethanol as the reaction solvent and regulated the growth of anatase TiO_2 to obtain TiO_2 with high {001} surface exposure, and added F^- to further reduce the surface energy of TiO_2. Through this method, the thickness of anatase TiO_2 nanosheets can be successfully reduced to ≈2.5 nm, side length ≈200 nm, and {001} plane accounting for 97%. Using Pt as a cocatalyst, TiO_2 nanosheets showed high activity (17.86 mmol h^{-1} g^{-1}) at UV (365 ± 10 nm) with an apparent quantum efficiency (QE) of 34.2%.

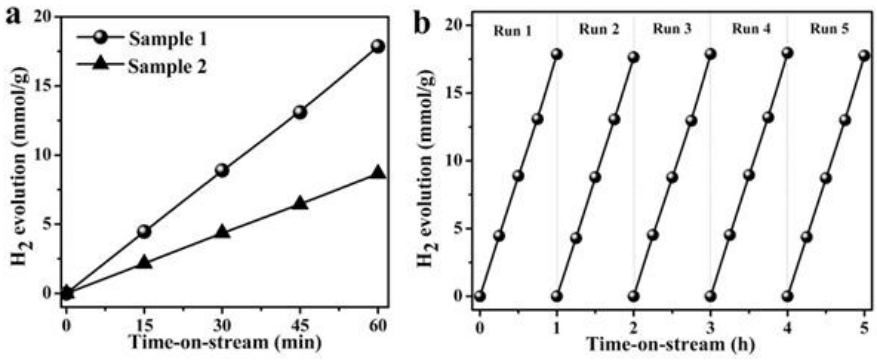

Figure 8. Ethanol was added during the synthesis of sample 1 and no ethanol in sample 2. (**a**) Photocatalytic hydrogen production of anatase TiO_2 nanosheets under UV, (**b**) Photocatalytic hydrogen production cycle experiment of sample 1 under UV. Reprinted with permission from [146].

Loading the oxidation or reduction cocatalyst on semiconductor surfaces is a broadly used and effective strategy, which can separate effectively photogenerated electrons and holes and generate surface redox reaction sites [147–150]. Although theoretically loading the oxidation or reduction cocatalyst simultaneously can enhance photocatalytic activity, in most cases, the cocatalyst will be randomly distributed on the surface of the semiconductor, which leads to a higher recombination rate of photogenerated electrons and holes [151]. Due to the limitations of traditional methods in preparing this type of photocatalyst, there have been few reports of success. Atomic layer deposition (ALD) is a new and effective method for the preparation of high dispersion loaded materials [152]. Jiankang Zhang et al. [153] (Figure 9) used the ALD method to modify Pt internally and CoO_x externally in surfaces of porous TiO_2 nanotubes with carbon nanotubes as template, and synthesized a new porous tubular CoO_x/TiO_2/Pt photocatalyst, which was successfully used in photocatalytic hydrogen production. The photogenerated electrons and holes flow inward and outward, respectively, in the porous titanium dioxide nanotubes. It can be seen that the highest activity was found when both Pt and CoO_x were loaded at the same time, which was higher than that when Pt and CoO_x were loaded alone.

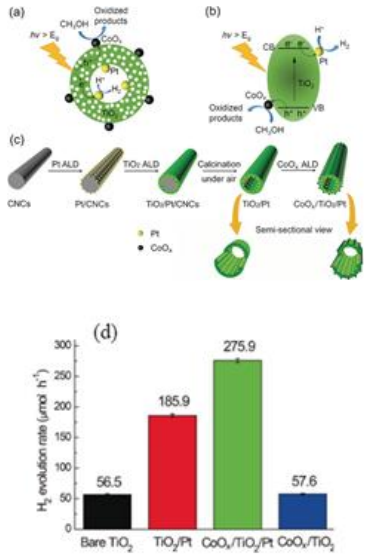

Figure 9. (**a**,**b**) The mechanism of photocatalytic hydrogen production by CoOx/TiO_2/Pt. (**c**) Synthetic process of CoO_x/TiO_2/Pt by atomic layer deposition (ALD). (**d**) Photocatalytic hydrogen production of different photocatalysts in a 15 vol% methanol–water solution under UV. Reprinted with permission from [153].

In addition to Pt, some other noble metals are used as cocatalysts or dopants to enhance the photoactivity of the semiconductor. Alenzi et al. [154] synthesized a TiO_2 nanofilm doped with Ag, and this composite film showed a greater hydrogen production activity with an average hydrogen production rate of 147.9 ± 35.5 μmol h^{-1} g^{-1} than TiO_2. Using calculations based on density functional theory (DFT), Mazheika et al. [155] found that Ag could modify the surface of anatase TiO_2, resulting in defects such as oxygen vacancy when Ag was introduced into the TiO_2 lattice [156]. With these vacancies, a transmission channel with high conductivity can be created, thereby effectively separating electrons from holes [157]. Yingfeng Xu et al. [158] developed a particularly simple and effective palladium catalytic strategy for hydrogenation of TiO_2. The point defects (Ti^{3+} and oxygen vacancy) in TiO_2 significantly narrow the band gap and improve the activity of TiO_2. In addition, due to the oxygen assistance, the autothermal effect generated during palladium-catalyzed hydrogenation induces a unique crystalline core/disordered shell structure, which is believed to prevent photogenerated electors and holes from recombination and is conducive to the cycling stability of TiO_2 after redox reduction. This simple and universal palladium catalytic hydrogenation method will open up new ways to produce inherent defects in oxides and greatly improve catalytic performance.

Non-metallic element doped TiO_2 has obvious advantages due to its unique characteristics of small ionic radius, high thermal stability, and few recombination centers. Studies have shown that N or S [159–161] doped TiO_2 can narrow the optical band gap and increase photocatalytic activity. Recently, a series of N-doped TiO_2 nanobelts have been reported by Shuchao Sun et al. [162]. The unique shape of the nanobelt provides well-defined nanostructures with (101) and (001) faces on exposed surfaces. The maximum hydrogen yield rate of these N-doped TiO_2 nanoribbon is 670 μmol$h^{-1}g^{-1}$, much higher than other values reported in the previous TiO_2 nanobelt conventional literature (only a few μmol $h^{-1}g^{-1}$). S doped TiO_2 was prepared by oxidative annealing of TiS_2 as reported by Umebayashi et al. [163]. At the annealing temperature of 600 °C, a part of TiS_2 was transformed to anatase TiO_2. The residual S atoms formed S-doped TiO_2 by the Ti–S bond. The S-doped energy band structure is calculated by the super-cell method. It was found that when TiO_2 mixed with S 3p increased the height of the valence band, it led to narrowing of the band gap. As the narrowing of the band gap is caused by the upward migration of valence bands, the conduction band remains unchanged, so S-doped TiO_2 can produce hydrogen in visible light.

In photocatalysis, TiO_2 can be combined with other semiconductors to extend the absorption wavelength range to the visible region and slow down electron-hole recombination [164,165].

Kim et al. [166] reported a new system using a TiO_2 photocatalyst loaded with Bi_2S_3 (Bi_2S_3/TiO_2). Bi_2S_3 particles are similar to the shape of a sea urchin, with a length of about 2–3 nm and a diameter of 15–20 nm. Compared with pure TiO_2 and Bi_2S_3, Bi_2S_3/TiO_2 composite material has enhanced hydrogen generation capacity in methanol/water (1:1) system.

Chai et al. [167] reported g–C_3N_4–Pt–TiO_2 nanocomposite was prepared by simple chemical adsorption and calcination. Through a series of characterization, it was found that the photocatalytic activity of the composites could be significantly improved. The photocurrent stability of g–C_3N_4–TiO_2 is about 1.5 times that of g–C_3N_4. Due to the synergistic effect

between Pt–TiO_2 and g–C_3N_4, the photogenerated electrons of g–C_3N_4 can transform to Pt–TiO_2, and the photogenerated electrons and holes can be effectively separated, which can effectively hinder the rapid recombination of photogenerated electrons and holes and improve the photocatalytic activity.

Some typical examples of improving photocatalytic activity are described above, which have given us great inspiration. In addition, Table 1 lists the basic methods commonly used in the literature to improve photocatalytic activity such as metal doping, non-metal doping, and composites. Through comparison, it can be seen that in the process of photocatalytic hydrogen production, due to the advantages of the nanosheet structure, most materials were synthesized into thinner nanosheets in order to seek rapid electron migration to the surface and therefore improve catalytic activity. The highest activities were Co (III)/TiO_2 and F–TiO_2, showing that metal and non-metal doping could significantly improve the photocatalytic activity. Doping is the simplest and easiest way to improve photocatalytic activity. In the process of composites, two or three semiconductors with suitable band structures are usually combined so that the photogenerated electrons can be separated effectively. However, due to the complexity of the implementation method, it is not conducive to large-scale industrial production.

Table 1. Summary of common methods to improve the photocatalytic hydrogen production activity of TiO_2.

Catalyst	Morphology	Reaction Conditions	Activity	Reference
S–TiO_2	Nanopillar	AM 1.5	163.9 μmol h^{-1} g^{-1}	[168]
F–TiO_2	Nanosheet	UV–Vis	18,270 μmol h^{-1} g^{-1}	[169]
TiO_2 @ReS_2	Nanorod	Visible light	1404 μmol h^{-1} g^{-1}	[170]
P/TiO_2(B)	Nanofiber	AM1.5	380 μmol $h^{-1}g^{-1}$	[171]
Ag/TiO_2	Nanosheet	UV–Vis	1.34 μmol cm^{-2} h^{-1}	[172]
Fe/Ni–TiO_2	Nanoparticle	Visible light	361.64 μmol h^{-1} g^{-1}	[173]
Co(Ⅲ)/TiO_2	Nanosheet	AM 1.5	20 mmol $h^{-1}g^{-1}$	[174]
TiO_2:Rh/Nb	Nanorod	UV–Vis	0.99 mmol g^{-1} h^{-1}	[175]
MoxS@TiO_2@Ti_3C_2	Nanosheet	AM 1.5	10,505.8 μmol $h^{-1}g^{-1}$	[176]
Au/TiO_2/SDA	Nanosheet	Visible light	264 μmol g^{-1} h^{-1}	[177]
C-TiO_2/g–C_3N_4	Nanosheet	Visible light	1409 μmol h^{-1} g^{-1}	[178]

4. Photocatalytic Dye Degradation

With the improvement in industrialization, the mass production rate of dyes has increased, so effective waste water treatment is needed [179]. Therefore, many methods have been developed to treat this apparent challenge, but these physical techniques (e.g., activated carbon adsorption and resin adsorption, reverse osmosis, extraction, ultrafiltration) simply transfer contaminants from one medium to another, causing secondary pollution. This usually requires further treatment of the absorbent or extractant, which increases the cost of the process. In recent years, extensive studies have been carried out on a wide range of synthetic dyes. Since 1972, when TiO_2 was first used for photocatalytic hydrogen production, photocatalysis has attracted much attention. Since the electron with energy generated by TiO_2 under light degraded the dyes, a series of catalysts were developed for the photocatalytic degradation of dyes. Among the different types of photocatalysts, photocatalytic oxidation assisted by titanium dioxide (TiO_2) has attracted much attention in recent years due to its non-toxicity, strong oxidation capacity, and long-term optical stability [180].

The introduction of carbon nanotubes (CNT) into nano-TiO_2 to prepare highly active photocatalyst has attracted the attention of many researchers [181–184]. These reports indicate that when decorated with CNT, the photocatalytic activity of TiO_2 can be observably enhanced. It has been indicated that CNT is an electron acceptor, hinders the recombination of electrons and holes, and increases the superficial area of TiO_2 and the number of active sites. Azzam et al. [185] successfully synthesized the nano-composite materials by CNT, TiO_2, and silver nanoparticles (AgNPs) for the photodegradation of dyes. The synthesized catalyst was modified with a cationic surfactant to increase the dispersion of TiO_2 and reduce the surface interaction (TiO_2@CNT/AgNPs/C10). The results of N_2 gas adsorption and desorption showed that the obtained material had a large specific surface area. Due to the co-modification of Ag nanoparticles and CNT, the TiO_2 composite had a lower band gap (2.25 eV). It is obvious from Figure 10 that TiO_2 @CNT/AgNPs/C10 had the highest catalytic activity.

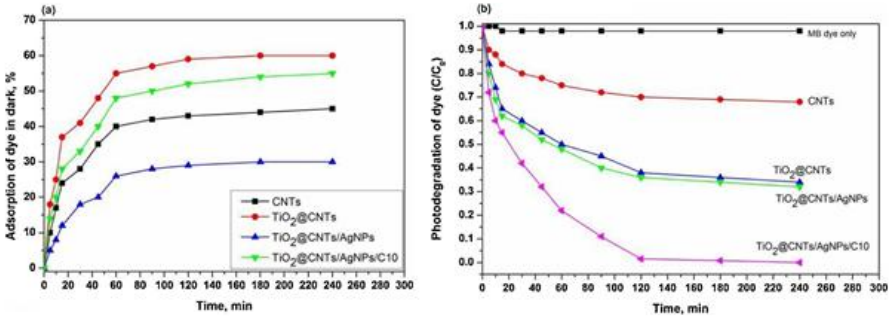

Figure 10. Degradation of methylene blue dye by (**a**) adsorption and (**b**) photodegradation under visible light [C_0 = 20 mg/L, catalyst dose = 0.5 g/L, pH = 5.8 and T = 25 °C]. Reprinted with permission from [185].

TiO_2 doping includes Au, Ag, Pt, and other noble metal nanoparticles (NPs) that can effectively promote the separation of photogenerated electrons and holes, and the noble metal can also act as an active site for the photocatalytic degradation of organic dyes [137,186]. In general, the smaller the size of NPs, the more active sites they provide [187]. However, the bonding properties between metals and semiconductors are largely dependent on the properties of ligands on the metal surface (organic ligands are often added to avoid NP aggregation in solution) and organic ligands on the metal surface form a physical barrier that prevents the reactants from spreading to the active site and the transfer of electrons from the nano-TiO_2 to the noble metal [188]. Haiguang Zhu et al. [189] synthesized a photocatalyst for TiO_2 nanoparticles (NPs) doped with gold nanoclusters (Au NCs), which are protected by per-6-thio-β-cyclodextrin (SH-β-SD).The use of SH-β-SD facilitates the formation of an interface between Au NCs and TiO_2, thus forming an effective photocatalyst and overcoming the disadvantages of organic ligands in the synthesis of traditional photocatalysts. The photocatalytic activity was evaluated by MO (Methyl Orange) degradation. As shown in Figure 11, TiO_2–Au NCs–β–CD exhibited higher photocatalytic activity for MO degradation under UV light than other composite materials. In particular, over 98% of the MO was degraded using TiO_2–Au NCs–β–CD within 10 min, while about 47% of the MO was degraded using TiO_2.

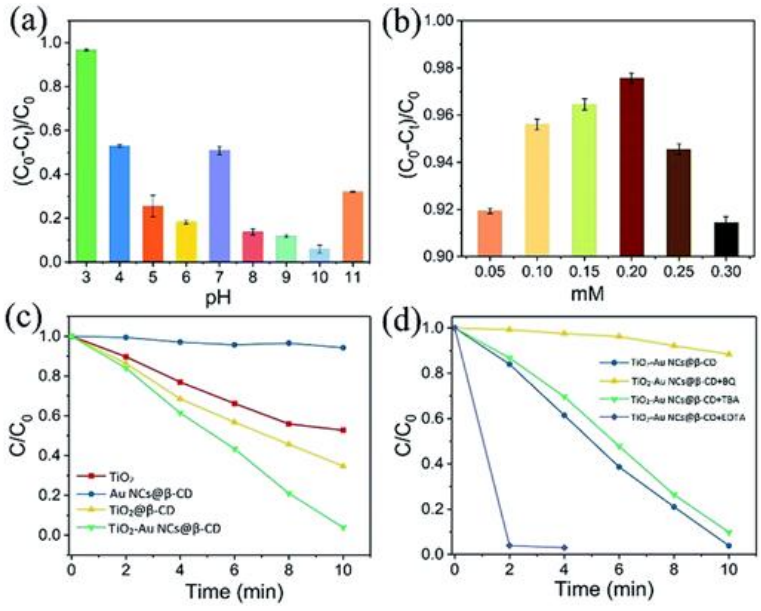

Figure 11. (a) Photodegradation efficiency of TiO_2–Au NCs@β-CD (t = 10 min) for MO at different solution pH. (b) Photodegradation efficiency of TiO_2–Au NCs@β-CD for MO (pH = 3), which was prepared by using different amounts of Au NCs@β-CD (t = 10 min). (c) Relative concentration (C/C0) versus time plot for the photodegradation of MO in the

presence of various amounts of catalysts under UV light. (d) Relative concentration (C/C0) versus time plot for the photodegradation of MO by TiO_2–Au NCs@β-CD in the presence of different kinds of scavengers. Reprinted with permission from [189].

Due to the high price of noble metals and the influence of organic ligands, the photocatalytic capacity of noble metals cannot be fully developed. Recently, monatomic catalysis has displayed great potential in improving photocatalytic activity and noble metal utilization [190–192]. Monatomic metal can improve more active sites and avoid the influence of organic ligands [193]. Tongzhou Xu et al. [194] synthesized a photocatalyst for TiO_2 nanofilms with atom Pt injection, and TiO_2 nanofilms exposed a {001} face (Figure 12). Photocatalytic degradation of acetamide under vacuum ultraviolet (VUV) and ultraviolet (UV) irradiation was used to evaluate the photocatalyst activity. Photocatalytic degradation showed high activity and stability. When the initial concentration was 500 ppb and 100 ppb, respectively, the degradation rate of acetamide reached 94.52% and 100% after 5 min of irradiation, which were 2.19 and 3.98 times of the nanoporous TiO_2.

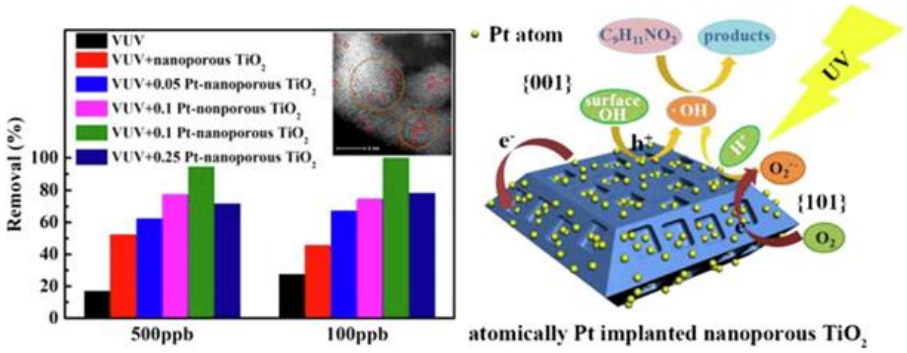

Figure 12(**a**) Photocatalytic degradation of dye activity within 0.5 min (**b**) Photocatalytic mechanism atomically Pt-nanoporous TiO_2 with exposed {001} facets under UV irradiation. Reprinted with permission from [194].

Nano-TiO_2 photocatalyst powders are easily agglomerated in solution and their activity is reduced. Furthermore, dispersion in solution makes recycling difficult. These defects limit the wide application of TiO_2 photocatalysis in industry [195,196]. Recently, it has been reported that nano-TiO_2 powder fixed on the supporting material can effectively solve the problem of agglomeration and circulation [197,198]. Yang Li et al. [199] successfully prepared a photocatalyst by loading TiO_2 nanoparticles on polymethyl methacrylate (PMMA) nanofibers through water treatment of electrospun PMMA nanofibers containing n-butanol titanium precursors at 135 °C (Figure 13). Under the irradiation of ultraviolet lamp, 0.1 g TiO_2@PMMA can completely degrade 100 mL MO in 50 min, which has a high photocatalytic activity. Moreover, TiO_2@PMMA could be separated from the reaction liquid by filtration and remained stable in five consecutive MO degradation cycles without obvious inactivation.

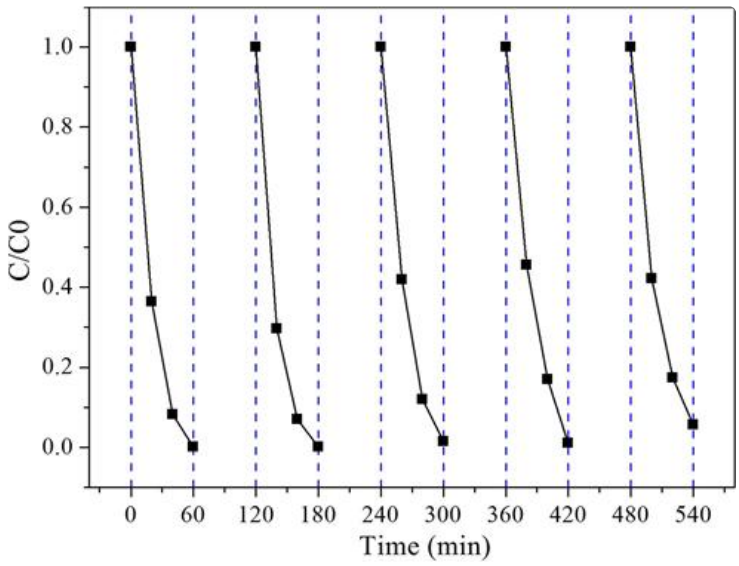

Figure 13. Cycle test of photocatalytic degradation of MO by TiO_2@PMMA ([MO] = 10 mg/L). Reprinted with permission from [199].

There have also been some studies to improve the activity of photocatalysts by simply doping TiO_2 with nonmetal or metal, which can be used for the degradation of dyes.

Alam U et al. [200] synthesized a Bi-doped TiO_2NT/graphene composite catalyst by the hydrothermal method. The synergic effect of Bi and graphene embedded in TiO_2 nanotubes promoted the interface charge transfer and improved the visible light efficiency. Wang Weikang et al. [201] synthesized a boron-doped TiO_2 (a/r adjustable) photocatalyst by the one-step roasting method. The electron transfer occurring in the two-phase interface is conducive to charge separation, and the charge trap is provided by the b-less electron structure, which improves the degradation capacity of atrazine. Xing Huan et al. [202] prepared a Ti^{3+} self-doped TiO_2 single crystal with oxygen vacancy as the electron trap. The results showed that the photodegradation activity of phenol increased significantly. Nair S B et al. [203] prepared self-doped TiO_2 nanotubes (TONT) by electrochemical reduction, introduced Ti^{3+} ions, and oxygen vacancy to reduce the band gap, and the degradation of methylene blue reached 97% under visible light irradiation.

Combination is also an easy way to improve the activity of nano-TiO_2 in the early stage by combining the appropriate semiconductor to improve the activity of the catalyst.

Liu Chao et al. [204] obtained graphene-like carbon plane grafted g–C_3N_4 by calcining, and then conjugated it with TiO_2 to construct a ternary heterostructure (carbon plane/g–C_3N_4/TiO_2), which can be extended to visible light absorption and degrade methylene blue (98.6%), tetracycline (94.0%), and norfloxacin (95.3%), and has good cyclic stability. The carbon plane of the graphene layer makes full contact with the ternary heterojunction, improves the efficiency of charge separation, and inhibits photocatalytic electron-hole pair recombination.

In addition to degrading dyes, TiO_2 is also used to degrade other pollutants such as antibiotics, heavy metals, and toxic gases. Pengzhao Ya et al. [205] reported that based on the hard-soft acid-base (HSAB) principle, TiO_2 was directly compounded with NH_2–UiO–66 to synthesize a TiO_2@NH_2–UiO–66 nanocomposite used for the photocatalytic degradation of styrene. Due to the porosity of MOF, the quaternary ammonium salt around TiO_2 can be well encapsulated, thereby prolonging its residence time at the photocatalytic active site and improving the activity. This method can form a good contact interface between TiO_2 and NH_2–UiO–66, and can effectively promote the separation of photogenerated electrons and holes. Compared with blank TiO_2 and NH_2–UiO–66, the degradation efficiency is significantly improved. The TiO_2@NH_2–UiO–66 photocatalyst has good stability, and the photocatalytic activity can last 600 min without obvious deactivation. Haibo Sheng et al. [206] prepared TiO_2@MIL-101 double-shell hollow particles for the photocatalytic degradation of H_2S, showing good activity. The conversion rate of hydrogen sulfide can reach up to 90.1%, which is obviously improved when compared with hollow and blank TiO_2. The reaction reached equilibrium in 60 min, which is a significant improvement compared to hollow TiO_2. Due to its excellent H_2S adsorption capacity, MIL-101 can significantly enhance the photocatalytic activity.

In addition to the above methods, Table 2 lists common ways to improve the degradation activity of photocatalytic dyes, which are similar to those in photocatalytic hydrogen production. Since the dyes have no energy level requirements for other applications, the implementation is relatively simple, and it can be seen that nanotubes and nanometers TiO_2 have advantages. From the perspective of activity, the $[Pt_3(CO)_6]_6^{2-}$–TiO_2 photocatalyst with noble metal Pt had the highest activity, but due to different degradation dyes and different final degradation rates, it was difficult to compare the difference in activity. From a rough perspective, TiO_2 doped with a noble metal such as Ag and Pt have a high activity, but has a high price. Transition metal doping showed higher activity than non-metal doping, showing an advantage in dye degradation. The composites showed high degradation rates, but it took a long time to degrade.

Table 2. Summary of common methods to improve TiO_2 photocatalytic dye degradation activity.

Catalysts	Morphology	Reaction Conditions	Catalyst dosage	Degradation Efficiency for Organic Dyes	Reference
Ag^0–TiO_2 nanosol	Nanoparticle	Visible light	50 mL	50 mL of 1×10^{-5} M RB, 90% in 4 h.	[207]
Ag–TiO_2	Nanotube	UVA(360nm)	NA	3 mL of 2.5×10^{-5} M AO7, 80% in 1 h	[208]
Au–TiO_2	Nanotube	UVA (360 nm)	NA	3 mL of 2.5×10^{-5} M AO7, 67% in 1 h	[208]

$Ag–In_2O_3–TiO_2$	Nanoparticle	UVB (313 nm)	1.67 g L^{-1}	90 mL of 25 mg L^{-1} RB, 100% in 45 min	[209]
$PtCl_4^{2-}–TiO_2$	Nanoparticle	Visible light	0.5 g L^{-1}	1 × 10^{-4} M RB, 90% in 2 h	[210]
$PtCl_6^{2-}–TiO_2$	Nanoparticle	UV–Vis	0.5 g L^{-1}	1 × 10^{-4} M RB, 100% in 20 min.	[210]
$[Pt_3(CO)_6]_6^{2-}–TiO_2$	Nanoparticle	UV–Vis	0.5 g L^{-1}	1 × 10^{-4} M RB, 100% in 15 min,	[210]
$Fe^{3+}–TiO_2$	Nanoparticle	Visible light	0.33 g L^{-1}	15 mL of 1 × 10^{-7} M SRB, 60.5% in 90 min	[211]
$Cu^{2+}–TIO_2$	Nanotube	UV	5 g L^{-1}	100 mL of 3 mg L^{-1} RB, 97.5% in 50 min.	[212]
Zn- TiO_2	Nanoparticle	UV	1 g L^{-1}	700 mL of 20 mg L^{-1} MO, 100% in 30 min.	[213]
$Cr^{3+}–TiO_2$	Nanotube	UV–Vis	0.5 g L^{-1}	100 mL of 20 mg L^{-1} MO, 96.9% in 3 h.	[214]
$C–TiO_2$	Nanotube	Artificial solar light	NA	97.3% of MB was achieved in 7 h.	[215]
$N–TiO_2$	Nanofilm	Visible light	NA	47.2% degradation of 30 mL of 20 mg L^{-1} MB	[216]
$B/N–TiO_2$	Nanoparticle	UV–Vis	NA	For RB, 86.5% in 1.5 h	[217]
$N/S–TiO_2$	Nanoparticle	UV	125 mg L^{-1}	800 mL of 10 mg L^{-1} MO, 88% in 1.5 h	[218]
$CdO/ZnO–TiO_2$	Nanofilm	Visible light	NA	500 mL of 100 mg L^{-1} textile blue azo dye, 100% in less than 2 h	[219]
RuO_2-SiO_2–TiO_2	Nanoparticle	UVA (350nm)	NA	4 mL of 5 mg L^{-1} MO, 100% in 2 h	[220]
$Ag/InVO_4–TiO_2$	Nanofilm	Visible light	NA	30 mL of 10 mg L^{-1} MO, 45% in 15 h.	[221]

5. Photocatalytic Reduction of Carbon Dioxide

Over the past few decades, the massive increase in CO_2 and the focus on energy supply are considered as the greatest challenges of this century. Converting CO_2 into renewable fuels through artificial photosynthesis has been considered as the best way to avoid both energy and environmental problems. Since Inoue [222] reported that semiconductors can reduce CO_2 in water, efforts have been made to build more efficient and environmentally friendly photocatalysts for CO_2 reduction. Up to now, most photocatalytic CO_2 reduction reactions using metal oxide semiconductor photocatalysts have been conducted under ultraviolet light or high power light irradiation, which is not suitable for practical production [223,224].

Photocatalytic reduction of CO_2 is similar to natural photosynthesis, in which plants convert CO_2 and H_2O to oxygen and carbohydrates under sunlight. In this process, solar energy is transformed and stored in the form of carbohydrates. It is a combination of water oxidation reaction and carbon dioxide reduction reaction (or CO_2 fixation reaction), involving light and dark reaction [225].

Due to the difference in obtained products, the difficulty of photocatalytic carbon dioxide reduction is different, but in order to improve the activity of the TiO_2 photocatalyst, most studies still adopt the simple strategy of metal or nonmetal doping or composites.

Andreu et al. [226] applied Mg loaded on the surface of TiO_2 (rutile type, anatase type, plate titanium type) nanoparticles for the photocatalytic reduction of CO_2, and the products were CO and CH_4. A little Mg can increase the concentration of Ti^{3+} (as an electron trap) and modified oxygen (as a hole trap), thereby reducing the charge recombination rate and increasing the activity of the catalyst. Tseng et al. [227] prepared a TiO_2-supported Cu catalyst by the sol-gel method, and orderly modified Cu distribution on the catalyst surface after post-treatment. Under ultraviolet light, the CH_3OH produced by the system was the greatest (1000 μmol·g^{-1}). Dispersed Cu(I) is considered as a key site for catalytic reduction. When Cu(I) changes to Cu(0) or its aggregates, the catalytic activity of the system decreases.

Xie et al. [228] supported different metal oxides (MgO, SrO, CaO, BaO, La_2O_3, Lu_2O_3) on the surface of a TiO_2/Pt catalyst. The study showed that the content of CH_4 for the MgO–TiO_2 composite was the highest. After the CO_2 molecule is absorbed in MgO, it becomes more concentrated, its structure is more unstable, and it is easier for it to participate in the reaction. Using TiO_2 (P25) as the framework, Li et al. [229] synthesized the CuO/TiO_2 catalyst (CuO mass fraction was 32%) by the dipping method. Using Na_2SO_3 as a sacrificial agent, the yield of reduced products CH_3OH and C_2H_5OH in water was 12.5 and 27.1 μmol/gk, respectively.

The most important problem limiting the widespread use of TiO_2 is the recombination of photogenerated electrons and holes. At present, the heterogeneous structure strategy has been proposed to inhibit recombination [230,231]. However, a single heterojunction had almost no effect on facilitating the separation of electrons and holes. Therefore, the construction of multiple heterostructures is necessary for the collaborative improvement of interface electron–hole separation and migration. Recently, a catalyst involving the design of an m–s junction with a p–n junction has been reported [232]. Compared with a single junction, the interaction of multiple heterojunctions results in the synergistic improvement of photocatalytic activity. As the distribution of the multiple heterogeneous structures on the surface of the photocatalyst is irregular, the effect of photogenerated electrons and holes is still poor. It has been reported that, on account of the difference in the electronic structure of anatase TiO_2 {101} and {001} faces, heterostructure can be carried out in different planes to separate the electrons and holes in space and aggregate on the {101} and {001} faces, respectively [223]. Therefore, Aiyun Meng et al. [233] designed one to construct the p–n junction with MnO_x on the TiO_2 {001} surface to facilitate hole migration from TiO_2 to the p-type semiconductor, and the m–n junction with Pt on the TiO_2 {101} surface for electron migration from TiO_2 to metal. The synthesized catalyst had a good hole–electron pair separation capability and a high photocatalytic activity. After three hours of light exposure, the maximum yield of CH_4 and CH_3OH reached 104 and 91 μmol m^{-2}, respectively, which was higher than that of pure TiO_2 and TiO_2/Pt, and the catalyst had good stability (Figure 14).

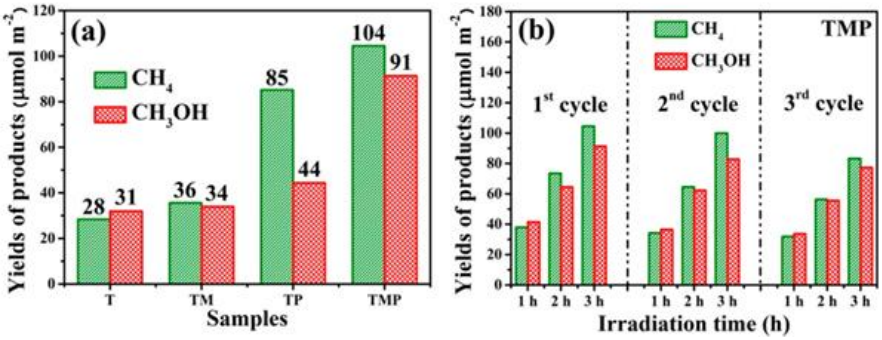

Figure 14. (**a**) Photocatalytic degradation of CO_2 activity of TiO_2 (T), TiO_2–Pt (TP), TiO_2–MnO_x (TM), and TiO_2–MnO_x–Pt (TMP) under UV–Vis for 3 h. (**b**) Photocatalytic cycling test of TMP. Reprinted with permission from [233].

Photocatalyst surface modification is an effective method to control the selectivity of photocatalytic degradation of carbon dioxide [234,235]. For example, the hydrophobic catalyst can inhibit the release reaction of hydrogen and improve the product selectivity of CO_2 conversion [236]. Sunil et al. [237] reported the successful synthesis of a Cu_2O/TiO_2 photocatalyst modified with taurine and ethylenediamine to degrade CO_2. Compared with the blank catalyst, taurine treatment improved the selectivity of CH_4 on the photocatalyst surface, while ethylenediamine treatment improved the selectivity of CO on the photocatalyst surface. Although the same Cu_2O/TiO_2 photocatalyst was used, the product

selectivity was significantly changed. Due to the difference in the number of electrons produced in the reaction, for example, different numbers of electrons are needed for CO_2 to degrade both CO and CH_4, and the ligand-treated samples (*TAU and *EDA) showed an overall enhanced photocatalytic activity. The selectivity of the products of CH_4 and CO was quite different from that of the blank photocatalyst. As shown in Figure 15, the CH_4 produced by *TAU was 2.4 times that of the blank sample, and the CO was 3.3 times less that of the blank sample; while the CO production rate of *EDA increased by more than 2.0 times, and the production of CH_4 was even less than that of the blank sample.

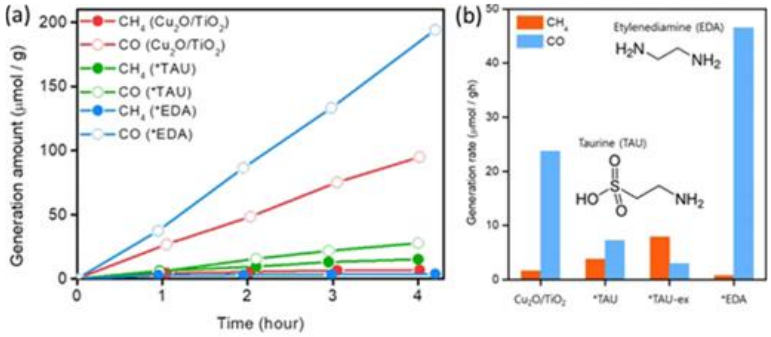

Figure 15. (**a**) CO and CH_4 are generated in the process of photocatalytic reduction of CO_2 for 4 h. (**b**) Photocatalytic degradation of CO_2 activity with different ligand treatment of TiO_2/Cu_2O. Reprinted with permission from [237].

Photocatalytic degradation of CO_2 is a multiple step process including adsorption, CO_2 activation, and CO_2 bond dissociation [238,239]. However, the reported photocatalytic composites for CO_2 reduction showed low CO_2 adsorption. Activated carbon fibers (ACFs) have recently been identified as an aussichtsreich large surface area base material that can effectively adsorb CO_2 [240,241]. Ajit et al. [242] synthesized a NiO/TiO_2 photocatalyst supported on an activated carbon fiber (ACF) (Figure 16). The layered porous structure and large surface area of ACF can better absorb CO_2. NiO/TiO_2 provides a catalytic surface for the photocatalytic degradation of CO_2 under visible light irradiation. The sol-gel prepared Ni^{2+} doped in TiO_2 to form Ti^{3+} and oxygen vacancy, and the doping changed the electronic structure of TiO_2, thus significantly improving the photoactivity of TiO_2 under visible light. The TiO_2 and NiO p–n equilibrium connection formed an internal electric field, which effectively improved the separation of photogenerated electrons and holes under visible light, making the photogenerated electrons move to the conductive band of n–TiO_2 and the holes to move to the valence band of p–NiO. Electron and hole pairs migrate to the surface of NiO/TiO_2, participate in the reduction and oxidation process, and catalyze the degradation of CO_2 to generate methanol. In the process of the photocatalytic degradation of CO_2 into methanol, the photocatalytic performance was relatively high. The yield of methanol generated under visible light for 2 h was 986.3 μmol g^{-1}. Even after 10 cycles, NiO/TiO_2/ACF was still stable.

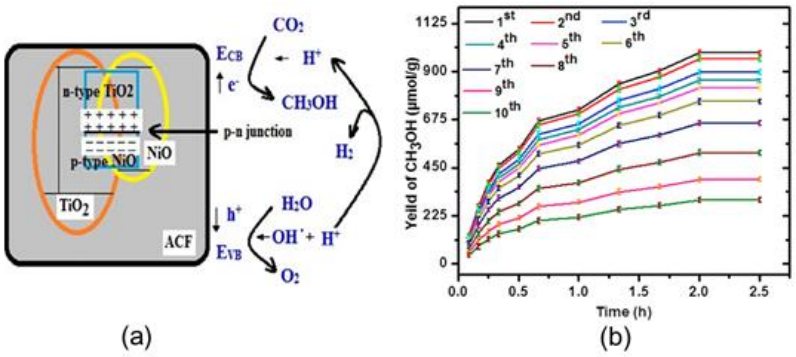

Figure 16(**a**) The mechanism of photocatalytic reduction of CO_2 into methanol. (**b**) Photocatalytic cycling test of NiO–TiO_2/ACF under visible light irradiation. Reprinted with permission from [242].

According to reports, graphene oxide (GO)/reduced graphene oxide (rGO) exhibits superior electron mobility, high specific surface area, and an adjustable band gap with semiconductor properties. Due to its semiconductor properties, Hsu et al. [243] reported that the reduced carbon dioxide was converted to methanol using GO as the photocatalysts. In this regard, there have been many reports on the functionalization of GO/rGO in the photocatalytic reduction of CO_2 into hydrocarbons under visible light [244–246]. Yalavarthi et al. [247] synthesized TiO_2 nanotubes coated with GO/rGO for the photocatalytic reduction of CO_2 (Figure 17). TiO_2 is wrapped in the GO/rGO layer, which also forms an interconnection bridge between adjacent nanotubes. This unique structure can favor photoproduction electron–hole separation and implement effective charge transfer, thus improving the photocatalytic activity. rGO/TiO_2 nanotubes showed the highest photocatalytic activity at 2 h of reaction rate of 760 μmol g^{-1}.

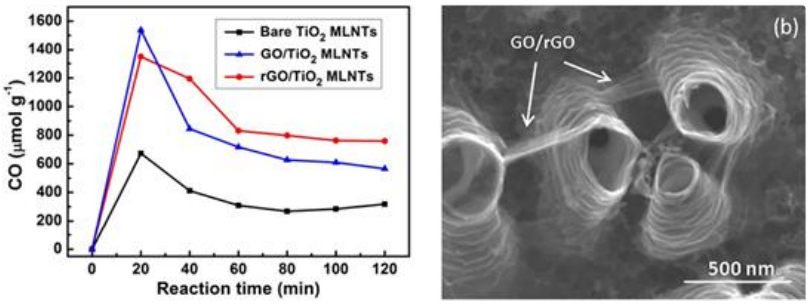

Figure 17. (**a**) The amount of carbon monoxide produced by the photocatalytic reduction of carbon dioxide from different composite materials. (**b**) Field Emission Scanning Electron Microscope (FESEM) images of rGO/TiO_2 nanotubes. Reprinted with permission from [247].

Table 3 lists the activity and morphology for photocatalytic CO_2 reduction. Different products of photocatalytic CO_2 reduction require different numbers of electrons, leading to different activity. Most of the morphologies are nanoparticles, and subsequent research should focus on changing the morphologies such as thinner structures with nanocrystals and nanowires, so that electrons can quickly migrate to the surface and participate in the reaction. The process of CO_2 degradation to CH_4 is the most difficult to achieve and requires the most electrons to participate in the reaction. In–TiO_2 exhibited the highest catalytic activity, demonstrating the superiority of metal doping in the catalytic formation of CH_4, and C–TiO_2 also had a high catalytic activity to generate HCOOH. At present, CO_2 degradation should focus on improving selectivity and generating CH_4 with high value-added. However, due to the high energy level of the reaction, such a target is difficult to achieve and the activity will not be particularly high.

Table 3. Summary of common methods to improve the photocatalytic reduction of the carbon dioxide activity of TiO_2.

Catalysts	Morphology	Reaction Conditions	Major Product	Product Yield	Reference
C–TiO_2	Nanoparticle	UV	HCOOH	438.996 μmol g^{-1} h^{-1}	[248]
N–TiO_2	Nanoparticles	UV–Vis	CH_3OH	10 μmol g^{-1} h^{-1}	[249]
N–TiO_2	Nanoparticle	Visible light	CH_4	0.155 μmol g^{-1} h^{-1}	[250]
V–TiO_2	Nanoparticle	Visible light	CH_3OH	1.15 μmol g^{-1} h^{-1}	[251]
Cr–TiO_2	Nanoparticle	Visible light	CH_3OH	0.25 μmol g^{-1} h^{-1}	[251]
Co–TiO_2	Nanoparticle	visible light	CH_3OH	1.63 μmol g^{-1} h^{-1}	[251]
In–TiO_2	Nanoparticle	UV	CH_4	243.75 μmol g^{-1} h^{-1}	[252]
Ag–TiO_2	Nanorod	UV	CH_4	2.64 μmol g^{-1} h^{-1}	[253]
Pt–TiO_2	Nanorod	UV	CH_4	2.5 μmol g^{-1} h^{-1}	[254]
Au–TiO_2	Nanoparticle	UV	CH_4	1.33 μmol g^{-1} h^{-1}	[255]
CdS/TiO_2	Nanoparticle	Visible light	CH_4	0.188 μmol g^{-1} h^{-1}	[256]
CuPc–TiO_2	Nanoparticle	UV–Vis	HCOOH	26.06 μmol g^{-1} h^{-1}	[257]

6. Photocatalytic Nitrogen Fixation

Ammonia (NH_3) is one of the most important products in today's chemical industry. It is the key raw material for the synthesis of various nitrogen-containing compounds [258]. Through the Haber–Bosch process invented in the early 20th century, NH_3 is produced by the hydrogenation of N_2, which consumes 2% global energy by humans each year and releases large amounts of greenhouse gases (CO_2 produced when fossil fuels are burned to provide heat) into the atmosphere [259]. Introducing solar or electrical energy instead of heat into nitrogen fixation reduces energy consumption and greenhouse gas emissions [260]. Among them, due to photocatalytic nitrogen fixation realized under mild conditions, it is considered as one of the most advanced ammonia synthesis methods. Schrauzer et al. [261] first reported TiO_2 as a photocatalyst for the reaction. Subsequently, it has been demonstrated that a variety of semiconductors including Fe_2O_3 [262], WO_3 [239], and BiOBr [263] have photocatalytic nitrogen fixation activities.

Photocatalytic nitrogen fixation is a newly developed branch in recent years, and there are few studies available. Currently, most studies are focused on doping TiO_2 to obtain higher performance. Of course, composites are also an appropriate strategy for nitrogen fixation. Weirong Zhao et al. [264] successfully prepared Fe-doped TiO_2 nanoparticles with high (1 0 1) face ratio by the two-step hydrothermal method. When ethanol is used as a hole-trapping agent, quantum yield can reach 18.27×10^{-2} m^{-2}, which is 3.84 times higher than blank TiO_2. Fe^{3+} ions uniformly mixed into anatase crystal and replaced Ti^{4+} in TiO_2 lattice can increase the density of charge carrier concentration to improve nitrogen fixation activity. Daimei Chen et al. [265] prepared three codoped nanoparticles of C-doped TiO_2, N-doped TiO_2, and C/N-doped TiO_2 by the simple sol-gel method. It is found that doping C and N atoms can inhibit the crystal growth of TiO_2. The influence of C doping is more obvious than that of N doping. N atoms can replace oxygen atoms in the lattice of anatase, while most C atoms are deposited on the surface. The results of nitrogen fixation showed that the C–N–TiO_2 nanomaterial showed the highest photocatalytic activity. Liu et al. [266] used a MXene derivative to synthesize the TiO_2@C/g–C_3N_4 heterojunction, and has rich surface defects, high electron donating ability, appropriate light capture, excellent charge transfer, and the strong ability of nitrogen activation. Excellent optical performance of the catalytic reduction of ammonia nitrogen is thus obtained, and NH_3 formation rate was 250.6 μmol h^{-1} g^{-1} under Vis.

The presence of defects in semiconductor photocatalysts has attracted extensive attention as an active site for reactions [267]. Recent studies have shown that a defective catalyst can be activated at a wavelength of 500 nm. It was proven that a thin catalyst could effectively improve the separation of the electron and hole [268]. Yunxuan Zhao et al. [269] synthesized Cu-doped TiO_2 nanosheets by using the Jahn–Teller distortion strategy, thus introducing a large number of oxygen vacancies and showing a wide range of solar absorption (Figure 18). The experiment showed that the TiO_2 nanosheets doped with Cu had a higher hole–electron separation efficiency and a higher nitrogen fixation activity. TiO_2 nanosheets doped with 6% Cu showed an activity of 78.9 μmol g^{-1} h^{-1} under full light irradiation, which was 1.54 and 0.72 μmol g^{-1} h^{-1}under 600 nm and 700 nm monochromatic excitation, respectively.

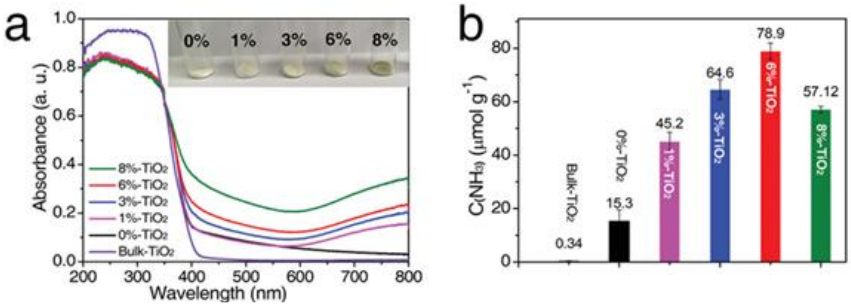

Figure 18. (a) UV-DRS of X %-TiO_2 nanosheets (X = 0, 1, 3, 6, 8) and Bulk-TiO_2 (the inset shows a photograph of the X %-TiO2 nanosheets). (**b**) Photocatalytic nitrogen fixation activity of TiO_2 with different doping concentrations under UV–Vis after 1 h. Reprinted with permission from [269].

Great efforts have been made to narrow the semiconductor band gap and reduce the photogenic electron–hole recombination rate [270–272]. Meanwhile, morphology adjustment has also been proven to be an effective means to improve photocatalytic activity [273]. For example, photocatalysts for core-shell structured nanoparticles exhibit the ability to modulate light propagation due to their unique morphology. Nanotubes with hollow structure and high specific surface area have higher light utilization due to multiple scattering effects. Shiqun Wu et al. [274] reported a photocatalyst with a high specific surface area and a large number of defects in hollow TiO_2 nanotubes. These two features in favor of the capture of light and photo-induced electron and hole separation, so as to promote the photocatalytic nitrogen fixation activity. First of all, the hollow is good for collecting light. Second, rich defects on TiO_2 nanotubes (oxygen vacancy and

Ti^{3+}) with larger surface area (344 m^2/g), are the active sites of nitrogen adsorption to improve the photocatalytic activity (Figure 19). Under the light, the titanium dioxide nanotubes show high and stable production of ammonia (106.6 $\mu molg^{-1} h^{-1}$).

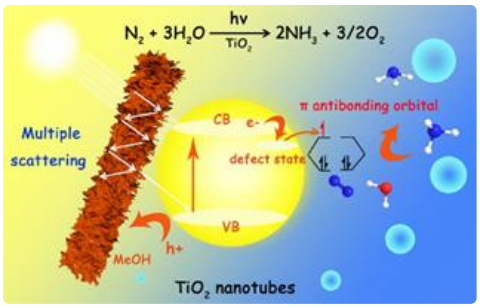

Figure 19. Photocatalytic nitrogen fixation mechanism by TiO_2 (B) nanotubes. Reprinted with permission from [274].

Recently, Li et al. [275] found that the oxygen vacancy (O_{vac}) in BiOBr nanosheets has the ability to absorb and reduce N_2 to NH_3. Similarly, O_{vac} in TiO_2 has the same capacity in the adsorption and reduction of N_2, which can be illustrated by the photocatalysis of N_2 under ultraviolet light by the TiO_2 photocatalyst containing O_{vac} [276]. However, when methods such as H_2 reduction are used to introduce O_{vac}, they cannot avoid the formation of body defects, which will cause photogenic electron–hole pair recombination [277]. Jiangpeng Wang et al. [278] reported that TiO_2 nanotubes with less oxygen vacancy were prepared by treating hydrogenated TiO_2 with dicyandiamide (DA) to repair the body defects. Electron spin resonance (ESR) results showed that the sample exhibited a strong paramagnetic peak due to a large number of oxygen vacancies and body defects after hydrogen treatment. However, after the DA treatment of the sample, only a very low ESR peak could be observed, indicating that a large number of body defects had been repaired, leaving only some oxygen vacancies. The NH_3 yield of the blank TiO_2 nanotubes for photocatalytic N_2 fixation was 0.14 $mmol \cdot L^{-1} \cdot h^{-1}$, the N_2 fixation performance of TiO_2–H_2–DA was greatly improved, and the generation rate of NH_3 reached 1.2 $mmol \cdot L^{-1} \cdot h^{-1}$(Figure 20). This value is more than eight times that of original TiO_2. It can be seen clearly that oxygen vacancy can improve the activity, but body defects will also be introduced. Appropriate treatment methods will effectively reduce the body defect and reserve part of the oxygen vacancy to improve the activity.

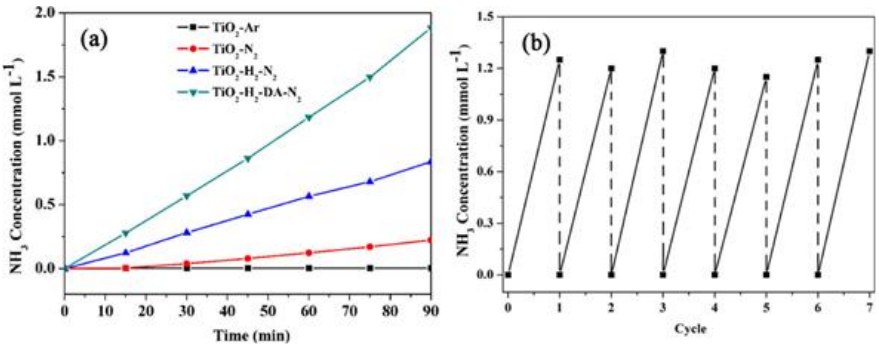

Figure 20. (**a**) Photocatalytic nitrogen fixation activities of different photocatalysts, (**b**) photocatalytic nitrogen fixation cycle activities of TiO_2–H_2–DA. Reprinted with permission from [278].

Due to the fact that photocatalytic nitrogen fixation is a newly developed field and is difficult to realize, the modification of TiO_2 is currently in the exploration stage. In addition to the above methods, only a few modification methods of TiO_2 have been reported in the literature. Table 4 lists the methods used to improve photocatalytic nitrogen fixation in some literatures. Due to the lack of references, it is difficult to compare the advantages of morphology. At present, the dopant activity of metals is relatively low. To obtain high dopant activity, a composite method is needed, but it is complex, and two suitable band semiconductors are required. The direction of photocatalytic nitrogen fixation is still in the exploratory stage, and the problem to be solved in the present research is to obtain high activity by using relatively easy means.

Table 4. Summary of common methods to improve the photocatalytic nitrogen fixation activity of TiO_2.

Catalyst	Morphology	Reaction Conditions	Product yield	Reference
Mg–TiO_2	Nanoparticle	UV–Vis	10.35 $\mu mol\ h^{-1}\ g^{-1}$	[279]

Cr–TiO_2	Nanoparticle	UV–Vis	2.12 μmol h^{-1} g^{-1}	[280]
V–TiO_2	Nanoparticle	UV–Vis	6.12 μmol h^{-1} g^{-1}	[281]
Ce–TiO_2	Nanoparticle	UV–Vis	4.25 μmol h^{-1} g^{-1}	[281]
Ru/TiO_2	Nanosheet	UV–Vis	3.32 μmol h^{-1} g^{-1}	[282]
Au/TiO_2	Nanotube	UV–Vis	1.04 μmol h^{-1} l^{-1}	[283]
RuO_2@TiO_2–MXene	Nanoparticle	UV–Vis	425 μmol l^{-1} g^{-1}	[284]

7. Conclusions

Due to its physical structure and good optical properties, titanium dioxide is considered to be a promising semiconductor photocatalyst, while nano-TiO_2 has the advantages of large specific surface area and more exposed active sites, so it has better performance than TiO_2. The important environmental applications of the nano-TiO_2 photocatalyst were highlighted in this review such as hydrogen production, dye degradation, CO_2 degradation, and nitrogen fixation. As reviewed here, a number of studies focused on making nano-TiO_2 active in the visible light region by various methods such as doping of metals or nonmetals, manufacturing defects, and compounding of other semiconductors. So far, the successful application of nano-TiO_2 photocatalysts in visible light has only been on a laboratory scale. Future research should focus on the use of novel nano-TiO_2 photocatalysts (doped nano-TiO_2 or composite nano-TiO_2) for large-scale application.

Reference

1. Midilli, A.; Dincer, I. Hydrogen as a renewable and sustainable solution in reducing global fossil fuel consumption. *J. Hydrog. Energy* **2008**, *33*, 4209–4222.
2. Nehring, R. Traversing the mountaintop: World fossil fuel production to 2050. *Trans. R. Soc. Lond. B Biol. Sci.* **2009**, *364*, 3067–3079.
3. Shafiee, S.; Topal, E. An econometrics view of worldwide fossil fuel consumption and the role of US. *Energy Policy* **2008**, *36*, 775–786.
4. Han, C.; Zhao, L.; Zhang, M.; Pan, L.; Liu, Z. Synthesis and Self-Cleaning Property of TiO_2 Thin Film Doping with Fe^{3+}, Al^{3+}, Ce^{3+} *J. Nanosci. Nanotechnol.* **2020**, *20*, 4084–4091.
5. Armaroli, N.; Balzani, V. The Legacy of Fossil Fuels. *Asian J.* **2011**, *6*, 768–784.
6. Baum, R. The Energy Commons—Part 2. *Eng. News* **2006**, *84*, 5.
7. Hardin, G.J.S. The tragedy of the commons. The population problem has no technical solution; it requires a fundamental extension in morality. *Science* **1969**, *162*, 1243–1248.
8. Bensalah, N.; Alfaro, M.A.Q.; Martínez-Huitle, C.A. Electrochemical treatment of synthetic wastewaters containing Alphazurine A dye. *Eng. J.* **2009**, *149*, 348–352.
9. Turhan, K.; Turgut, Z. Decolorization of direct dye in textile wastewater by ozonization in a semi-batch bubble column reactor. *Desalination* **2009**, *242*, 256–263.
10. Gosetti, F.; Gianotti, V.; Angioi, S.; Polati, S.; Marengo, E.; Gennaro, M.C. Oxidative degradation of food dye E133 Brilliant Blue FCF: Liquid chromatography–electrospray mass spectrometry identification of the degradation pathway. *Chromatogr. A* **2004**, *1054*, 379–387.
11. Konstantinou, I.K.; Albanis, T.A. TiO_2-assisted photocatalytic degradation of azo dyes in aqueous solution: Kinetic and mechanistic investigations: A review. *Catal. B* **2004**, *49*, 1–14.
12. Ajmal, A.; Majeed, I.; Malik, R.N.; Idriss, H.; Nadeem, M.A. Principles and mechanisms of photocatalytic dye degradation on TiO_2 based photocatalysts: A comparative overview. *RSC Adv.* **2014**, *4*, 37003–37026.
13. Anliker, R. Ecotoxicology of dyestuffs—A joint effort by industry. *Environ. Saf.* **1979**, *3*, 59–74.
14. Jena, K.L.; Studies, I. A bibliometric analysis of the journal 'Indian Journal of Fibre and Textile Research, 1996-2004'. *Libr. Sci. Doc.* **2006**, *53*, 22–30.
15. Nohynek, G.; Hueber-Becker, F.; Meuling, W.; Dufour, E.; Bolt, H.; deBie, A. Occupational exposure of hairdressers to [14C]-para-phenylenediamine-containing oxidative hair dyes. *Lett.* **2007**, *172*, S30–S31.
16. Cassano, A.; Molinari, R.; Romano, M.; Drioli, E. Treatment of aqueous effluents of the leather industry by membrane processes: A review. *Membr. Sci.* **2001**, *181*, 111–126.

17. Crini, G. Non-conventional low-cost adsorbents for dye removal: A review. *Technol.* **2006**, *97*, 1061–1085.
18. Wróbel, D.; Boguta, A.; Ion, R.M. Mixtures of synthetic organic dyes in a photoelectrochemical cell. *Photochem. Photobiol. A Chem.* **2001**, *138*, 7–22.
19. Albano, G.; Aronica, L.A.; Biver, T.; Detti, R.; Pucci, A. Tris-Ethynylphenyl-amine Fluorophores: Synthesis, Characterisation and Test of Performances in Luminescent Solar Concentrators. *ChemistrySelect* **2018**, *3*, 1749–1754.
20. Albano, G.; Colli, T.; Nucci, L.; Charaf, R.; Biver, T.; Pucci, A.; Aronica, L.A. Synthesis of new bis 1-(thiophenyl)propynones as potential organic dyes for colorless luminescent solar concentrators (LSCs). *Dyes Pigment.* **2020**, *174*, 108100.
21. Albano, G.; Colli, T.; Biver, T.; Aronica, L.A.; Pucci, A. Photophysical properties of new p-phenylene- and benzodithiophene-based fluorophores for luminescent solar concentrators (LSCs). *Dyes Pigment.* **2020**, *178*, 108368.
22. Bak, T.; Nowotny, J.; Rekas, M.; Sorrell, C.C. Photo-Electrochemical Hydrogen Generation from Water Using Solar Energy. Materials-Related Aspects. *J. Hydrog. Energy* **2002**, *27*, 991–1022.
23. Fujishima, A.; Honda, K. Electrochemical Photolysis of Water at a Semiconductor Electrode. *Nature* **1972**, *238*, 37–38.
24. Nagaveni, K.; Sivalingam, G.; Hedge, M.S.; Madras, G. Solar photocatalytic degradation of dyes: High activity of combustion synthesized nano TiO_2. *Catal. B* **2004**, *48*, 83–93.
25. Cong, Y.; Zhang, J.; Chen, F.; Anpo, M.; He, D. Preparation, photocatalytic activity, and mechanism of Nano-TiO_2 co-doped with nitrogen and iron (III). *Phys. Chem. C* **2007**, *111*, 10618–10623.
26. Macwan, D.P.; Dave, P.N.; Chaturvedi, S. A review on nano-TiO_2 sol-gel type syntheses and its applications. *Mater. Sci.* **2011**, *46*, 3669–3686.
27. Chen, S.; Liu, W.; Zhang, S.; Chen, Y. Preparation and activity evaluation of relative p-n junction photocatalyst Co-TiO_2/TiO_2. *Sol-Gel Sci. Technol.* **2010**, *54*, 258–267.
28. Tong, C.; Yoon, S.F.; Wang, L. Large size self-assembled quantum rings: Quantum size effect and modulation on the surface diffusion. *Nanoscale Res. Lett.* **2012**, *7*, 520.
29. Ohno, T.; Numakura, K.; Itoh, H.; Suzuki, H.; Matsuda, T. Control of the quantum size effect of TiO_2–SiO_2 hybrid particles. *Lett.* **2009**, *63*, 1737–1739.
30. Xue, X.; Ji, W.; Mao, Z.; Mao, H.; Wang, Y.; Wang, X.; Ruan, W.; Zhao, B.; Lombardi, J.R. Raman Investigation of Nanosized TiO_2: Effect of Crystallite Size and Quantum Confinement. *Phys. Chem. C* **2012**, *116*, 8792–8797.
31. Chen, Q.; Tong, R.; Chen, X.; Xue, Y.; Xie, Z.; Kuang, Q.; Zheng, L. Ultrafine ZnO quantum dot-modified TiO_2 composite photocatalysts: The role of the quantum size effect in heterojunction-enhanced photocatalytic hydrogen evolution. *Sci. Technol.* **2018**, *8*, 1296–1303.
32. Efstathiou, P.; Xu, X.; Menard, H.; Irvine, J.T.S. An investigation of crystal structure, surface area and surface chemistry of strontium niobate and their influence on photocatalytic performance. *Dalton Trans.* **2013**, *42*, 7880–7887.
33. Xie, Y.P.; Wang, G.S. Visible light responsive porous Lanthanum-doped Ag_3PO_4 photocatalyst with high photocatalytic water oxidation activity. *Colloid Interface Sci.* **2014**, *430*, 1–5.
34. Fan, X.-X.; Yu, T.; Zhang, L.-Z.; Chen, X.-Y.; Zou, Z.-G. Photocatalytic degradation of acetaldehyde on mesoporous TiO_2: Effects of surface area and crystallinity on the photocatalytic activity. *J. Chem. Phys.* **2007**, *20*, 733–738.
35. Kim, H.J.; Shul, Y.G.; Han, H.S. Photocatalytic properties of silica-supported TiO_2. *Catal.* **2005**, *35*, 287–293.
36. Mao, Z.; Vang, H.; Garcia, A.; Tohti, A.; Stokes, B.J.; Nguyen, S.C. Carrier Diffusion-The Main Contribution to Size-Dependent Photocatalytic Activity of Colloidal Gold Nanoparticles. *ACS Catal.* **2019**, *9*, 4211–4217.
37. Charanpahari, A.; Umare, S.S.; Sasikala, R. Effect of Ce, N and S multi-doping on the photocatalytic activity of TiO_2. *Surf. Sci.* **2013**, *282*, 408–414.
38. Drmosh, Q.A.; Hezam, A.; Hossain, M.K.; Qamar, M.; Yamani, Z.H.; Byrappa, K. A novel Cs_2O-Bi_2O_3-TiO_2-ZnO heterostructure with direct Z-Scheme for efficient photocatalytic water splitting. *Int.* **2019**, *45*, 23756–23764.
39. Wang, T.; Wei, J.; Shi, H.; Zhou, M.; Zhang, Y.; Chen, Q.; Zhang, Z. Preparation of electrospun Ag/TiO_2 nanotubes with enhanced photocatalytic activity based on water/oil phase separation. *E Low Dimens. Syst. Nanostruct.* **2017**, *86*, 103–110.
40. Ohno, T.; Akiyoshi, M.; Umebayashi, T.; Asai, K.; Mitsui, T.; Matsumura, M. Preparation of S-doped TiO_2 photocatalysts and their photocatalytic activities under visible light. *Water Sci. Technol.* **2004**, *265*, 115–121.
41. Li, D.; Haneda, H.; Hishita, S.; Ohashi, N. Visible-Light-Driven N−F−Codoped TiO_2 1. Synthesis by Spray Pyrolysis and Surface Characterization. *Chem. Mater.* **2005**, *17*, 2588–2595.
42. Wang, C.Y.; Bttcher, C.; Bahnemann, D.W.; Dohrmann, J.K. A comparative study of nanometer sized Fe(III)-doped TiO_2 photocatalysts: Synthesis, characterization and activity. *Mater. Chem. A* **2003**, *5*, 11143.
43. Zhou, Q.; Fang, Z.; Li, J.; Wang, M. Applications of TiO_2 nanotube arrays in environmental and energy fields: A review. *Microporous Mesoporous Mater.* **2015**, *202*, 22–35.
44. Wang, Y.; He, Y.; Lai, Q.; Fan, M. Review of the progress in preparing nano TiO_2: An important environmental engineering material. *Environ. Sci.* **2014**, *26*, 2139–2177.

45. Park, H.; Park, Y.; Kim, W.; Choi, W. Surface modification of TiO_2 photocatalyst for environmental applications. *Photochem. Photobiol. C* **2013**, *15*, 1–20.
46. Daghrir, R.; Drogui, P.; Robert, D. Modified TiO_2 for Environmental Photocatalytic Applications: A Review. *Eng. Chem. Res.* **2013**, *52*, 3581–3599.
47. Pelaez, M.; Nolan, N.; Pillai, S.; Seery, M.; Falaras, P.; Kontos, A.; Dunlop, P.; Hamilton, J.; Byrne, J.; O'Shea, K.; et al. A Review on the Visible Light Active Titanium Dioxide Photocatalysts for Environmental Applications. *Catal. B* **2012**, *125*, 331–349.
48. Nolan, N.T.; Seery, M.K.; Pillai, S.C. Spectroscopic Investigation of the Anatase-to-Rutile Transformation of Sol−Gel-Synthesized TiO_2 *J. Phys. Chem. C* **2009**, *113*, 16151–16157.
49. Curnan, M.T.; Kitchin, J.R. Investigating the Energetic Ordering of Stable and Metastable TiO_2 Polymorphs Using DFT+U and Hybrid Functionals. *Phys. Chem. C* **2015**, *119*, 21060–21071.
50. Hashimoto, K.; Irie, H.; Fujishima, A. TiO_2 Photocatalysis: A Historical Overview and Future Prospects. *J. Appl. Phys.* **2005**, *44*, 8269–8285.
51. Zhang, J.; Zhou, P.; Liu, J.; Yu, J. New understanding of the difference of photocatalytic activity among anatase, rutile and brookite TiO_2. *PCCP* **2014**, *16*, 20382–20386.
52. Tahir, M.; Amin, N.S. Advances in visible light responsive titanium oxide-based photocatalysts for CO_2 conversion to hydrocarbon fuels. *Energy Convers. Manag.* **2013**, *76*, 194–214.
53. Chen, W.-T.; Chan, A.; Al-Azri, Z.H.N.; Dosado, A.G.; Nadeem, M.A.; Sun-Waterhouse, D.; Idriss, H.; Waterhouse, G.I.N. Effect of TiO_2 polymorph and alcohol sacrificial agent on the activity of Au/TiO_2 photocatalysts for H2 production in alcohol–water mixtures. *Catal.* **2015**, *329*, 499–513.
54. Wen, J.; Xie, J.; Chen, X.; Li, X. A review on g-C_3N_4-based photocatalysts. *Surf. Sci.* **2017**, *391*, 72–123.
55. Zhu, C.; Liu, C.; Zhou, Y.; Fu, Y.; Guo, S.; Li, H.; Zhao, S.; Huang, H.; Liu, Y.; Kang, Z. Carbon dots enhance the stability of CdS for visible-light-driven overall water splitting. *Catal. B* **2017**, *216*, 114–121.
56. Sang, L.; Lin, J.; Zhao, Y. Preparation of carbon dots/TiO_2 electrodes and their photoelectrochemical activities for water splitting. *J. Hydrog. Energy* **2017**, *42*, 12122–12132.
57. Lin, C.-J.; Kao, L.-C.; Huang, Y.; Bañares, M.A.; Liou, S.Y.-H. Uniform deposition of coupled CdS and CdSe quantum dots on ZnO nanorod arrays as electrodes for photoelectrochemical solar water splitting. *J. Hydrog. Energy* **2015**, *40*, 1388–1393.
58. Kang, S.H.; Lee, S.-Y.; Gang, M.G.; Ahn, K.-S.; Kim, J.H. Bifunctional Effects of CdSe Quantum Dots and Nb_2O_5 Interlayer for ZnO Nanorods-based Photoelectrochemical Water-Splitting Cells. *Acta* **2014**, *133*, 262–267.
59. Azimirad, R.; Safa, S.; Ebrahimi, M.; Yousefzadeh, S.; Moshfegh, A.Z. Photoelectrochemical activity of graphene quantum dots/hierarchical porous TiO_2 *J. Alloys Compd.* **2017**, *721*, 36–44.
60. Majumder, T.; Mondal, S.P. Graphene quantum dots as a green photosensitizer with carbon-doped ZnO nanorods for quantum-dot-sensitized solar cell applications. *Mater. Sci.* **2019**, *42*, 65.
61. Formo, E.; Lee, E.; Campbell, D.; Xia, Y. Functionalization of Electrospun TiO_2 Nanofibers with Pt Nanoparticles and Nanowires for Catalytic Applications. *Nano Lett.* **2008**, *8*, 668–672.
62. Yu, Y.; Xu, D. Single-crystalline TiO_2 nanorods: Highly active and easily recycled photocatalysts. *Catal. B* **2007**, *73*, 166–171.
63. Kumaresan, L.; Mahalakshmi, M.; Palanichamy, M.; Murugesan, V. Synthesis, Characterization, and Photocatalytic Activity of Sr^{2+} Doped TiO_2 *Ind. Eng. Chem. Res.* **2010**, *49*, 1480–1485.
64. Zhang, K.; Zhou, W.; Chi, L.; Zhang, X.; Jiang, Z.J.C. Black N/H-TiO_2 Nanoplates with a Flower-Like Hierarchical Architecture for Photocatalytic Hydrogen Evolution. *ChemSusChem* **2016**, *9*, 2841–2848.
65. Tang, Y.; Wee, P.; Lai, Y.; Wang, X.; Gong, D.; Kanhere, P.; Lim, T.; Dong, Z.; Chen, Z. Hierarchical TiO_2 Nanoflakes and Nanoparticles Hybrid Structure for Improved Photocatalytic Activity. *Phys. Chem. C* **2012**, *116*, 2772–2780.
66. Sauvage, F.; Fonzo, F.D.; Bassi, A.L.; Casari, C.S.; Graetzel, M.J.N.L. Hierarchical TiO_2 Photoanode for Dye-Sensitized Solar Cells. *Nano Lett.* **2010**, *10*, 2562–2567.
67. Macak, J.M.; Albu, S.P.; Schmuki, P. Towards ideal hexagonal self-ordering of TiO_2 *Phys. Status Solidi RRL* **2007**, *1*, 181–183.
68. Fang, W.Q.; Zhou, J.Z.; Liu, J.; Chen, Z.G.; Yang, C.; Sun, C.H.; Qian, G.R.; Zou, J.; Qiao, S.Z.; Yang, H.G. Hierarchical Structures of Single-Crystalline Anatase TiO_2 Nanosheets Dominated by {001} Facets. *Eur. J.* **2011**, *17*, 1423–1427.
69. Li, H.; Bian, Z.; Zhu, J.; Zhang, D.; Li, G.; Huo, Y.; Li, H.; Lu, Y. Mesoporous Titania Spheres with Tunable Chamber Stucture and Enhanced Photocatalytic Activity. *Am. Chem. Soc.* **2007**, *129*, 8406–8407.
70. Kondo, Y.; Yoshikawa, H.; Awaga, K.; Murayama, M.; Mori, T.; Sunada, K.; Bandow, S.; Iijima, S. Preparation, Photocatalytic Activities, and Dye-Sensitized Solar-Cell Performance of Submicron-Scale TiO_2 Hollow Spheres. *Langmuir* **2008**, *24*, 547–550.

71. Chen, S.; Yu, M.; Han, W.P.; Yan, X.; Liu, Y.C.; Zhang, J.C.; Zhang, H.D.; Yu, G.F.; Long, Y.Z. Electrospun anatase TiO_2 nanorods for flexible optoelectronic devices. *RSC Adv.* **2014**, *4*, 46152–46156.
72. Roy, P.; Berger, S.; Schmuki, P. TiO_2 Nanotubes: Synthesis and Applications. *Chem. Int. Ed.* **2011**, *50*, 2904–2939.
73. Choi, W.; Termin, A.; Hoffmann, M.R. The Role of Metal Ion Dopants in Quantum-Sized TiO_2: Correlation between Photoreactivity and Charge Carrier Recombination Dynamics. *Phys. Chem.* **1994**, *98*, 13669–13679.
74. Sclafani, A.; Herrmann, J.M. Comparison of the Photoelectronic and Photocatalytic Activities of Various Anatase and Rutile Forms of Titania in Pure Liquid Organic Phases and in Aqueous Solutions. *Phys. Chem.* **1996**, *100*, 13655–13661.
75. Chen, X.; Mao, S.S. Titanium Dioxide Nanomaterials: Synthesis, Properties, Modifications, and Applications. *Rev.* **2007**, *107*, 2891–2959.
76. Chen, X.; Shen, S.; Guo, L.; Mao, S.S. Semiconductor-based Photocatalytic Hydrogen Generation. *Rev.* 2010, 110, 6503-6570.
77. Zhang, T.; Oyama, T.; Aoshima, A.; Hidaka, H.; Zhao, J.; Serpone, N. Photooxidative N-demethylation of methylene blue in aqueous TiO_2 dispersions under UV irradiation. *Photochem. Photobiol. A* **2001**, *140*, 163–172.
78. Soria, J.; Conesa, J.C.; Augugliaro, V.; Palmisano, L.; Schiavello, M.; Sclafani, A. ChemInform Abstract: Dinitrogen Photoreduction to Ammonia over Titanium Dioxide Powders Doped with Ferric Ions. *Phys. Chem.* **1991**, *95*, 274–282.
79. Yu, J.C.; Yu, J.; Ho, W.; Jiang, Z.; Zhang, L. Effects of F- Doping on the Photocatalytic Activity and Microstructures of Nanocrystalline TiO_2 *ChemInform* **2002**, *33*, 12.
80. Wang, D.; Hisatomi, T.; Takata, T.; Pan, C.; Katayama, M.; Kubota, J.; Domen, K. ChemInform Abstract: Core/Shell Photocatalyst with Spatially Separated Co-Catalysts for Efficient Reduction and Oxidation of Water. *Angew. Int. Ed. Engl.* **2014**, *45*, 11252–11256.
81. Engweiler, J.; Harf, J.; Baiker, A. WOx/TiO_2Catalysts Prepared by Grafting of Tungsten Alkoxides: Morphological Properties and Catalytic Behavior in the Selective Reduction of NO by NH_3. *Catal.* **1996**, *159*, 259–269.
82. Vinodgopal, K.; Kamat, P.V. Enhanced Rates of Photocatalytic Degradation of an Azo Dye Using SnO_2/TiO_2 Coupled Semiconductor Thin Films. *Sci. Technol.* **1995**, *29*, 841–845.
83. Maira, A.J.; Yeung, K.L.; Lee, C.Y.; Yue, P.L.; Chan, C.K. Size Effects in Gas-Phase Photo-oxidation of Trichloroethylene Using Nanometer-Sized TiO_2 *J. Catal.* **2000**, *192*, 185–196.
84. Liu, P.; Kang, B.X.; Cao, X.G.; Huang, J.L.; Yin, B.; Gu, H.C. Interaction of precipitation and recrystallization in rapidly solidified Cu-Cr-Zr-Mg alloy. *Acta Metall. Sin. (Engl. Lett.)* **1999**, *12*, 273–275.
85. Tashbaeva, R.E.; Hwang, D.N.; Song, G.S.; Choi, N.H.; Lee, J.H.; Lyoo, Y.S.; Lee, S.J.; Jung, D.I.; Kim, H.Y.; Sur, J.H. Cellular Characterization of Multidrug Resistance P-glycoprotein, Alpha Fetoprotein, and Neovascular Endothelium-Associated Antigens in Canine Hepatocellular Carcinoma and Cirrhotic Liver. *Pathol.* **2007**, *44*, 600–606.
86. Asahi, R.; Morikawa, T.; Ohwaki, T.; Aoki, K.; Taga, Y. Visible-Light Photocatalysis in Nitrogen-Doped Titanium Oxides. *Science* **2001**, *293*, 269–271.
87. Pan, X.; Yang, M.-Q.; Fu, X.; Zhang, N.; Xu, Y.-J. Defective TiO_2 with oxygen vacancies: Synthesis, properties and photocatalytic applications. *Nanoscale* **2013**, *5*, 3601.
88. Zhu, R.X.; Potts, R.; Pan, Y.X.; Lü, L.Q.; Yao, H.T.; Deng, C.L.; Qin, H.F. Paleomagnetism of the Yuanmou Basin near the southeastern margin of the Tibetan Plateau and its constraints on late Neogene sedimentation and tectonic rotation. *Earth Planet. Sci. Lett.* **2008**, *272*, 97–104.
89. Niu, P.; Yin, L.C.; Yang, Y.Q.; Liu, G.; Cheng, H.M. Increasing the Visible Light Absorption of Graphitic Carbon Nitride (Melon) Photocatalysts by Homogeneous Self-Modification with Nitrogen Vacancies. *Mater.* **2014**, *26*, 8046–8052.
90. Hu, L.; Jian, Y.; Liao, M.; Xiang, H.; Gong, X.; Zhang, L.; Fang, X. An Optimized Ultraviolet-A Light Photodetector with Wide-Range Photoresponse Based on ZnS/ZnO Biaxial Nanobelt. *Mater.* **2012**, *24*, 2305–2309.
91. Zheng, L.R.; Zheng, Y.H.; Chen, C.Q.; Zhan, Y.Y.; Lin, X.Y.; Zheng, Q.; Wei, K.M.; Zhu, J.F. Network structured SnO_2/ZnO heterojunction nanocatalyst with high photocatalytic activity. *Chem.* **2009**, *48*, 1819–1825.
92. Smith, W.; Zhao, Y.P. Superior photocatalytic performance by vertically aligned core–shell TiO_2/WO_3 nanorod arrays. *Commun.* **2009**, *10*, 1117–1121.
93. Yang, M.; Hu, S.; Li, F.; Fan, Z.; Wang, F.; Liu, D.; Gui, J. The influence of preparation method on the photocatalytic performance of g-C_3N_4/WO_3 composite photocatalyst. *Int.* **2014**, *40*, 11963–11969.
94. Zhao, F.; Lu, Q.; Liu, S. Preparation and characterization of In_2O_3/ZnO heterostructured microbelts by sol–gel combined with electrospinning method. *Sol-Gel Sci. Technol.* **2014**, *69*, 357–363.
95. Shifu, C.; Wei, Z.; Wei, L.; Huaye, Z.; Xiaoling, Y. Preparation, characterization and activity evaluation of p–n junction photocatalyst p-$CaFe_2O_4$/n-ZnO. *Eng. J.* **2009**, *155*, 466–473.
96. Liu, Y.; Li, G.; Mi, R.; Deng, C.; Gao, P. An environment-benign method for the synthesis of p-NiO/n-ZnO heterostructure with excellent performance for gas sensing and photocatalysis. *Actuators* **2014**, *B191*, 537–544.
97. Chen, S.; Wei, Z.; Wei, L.; Zhang, S.J. Preparation, characterization and activity evaluation of p − n junction photocatalyst p-ZnO/n-TiO_2. *Hazard. Mater.* **2009**, *50*, 1415–1423.

98. Zou, Z.; Xie, C.; Zhang, S.; Yang, C.; Zhang, G.; Li, Y. CdS/ZnO nanocomposite film and its enhanced photoelectric response to UV and visible lights at low bias. *Actuators* **2013**, *B188*, 1158–1166.
99. Liu, Z.; Zhao, Z.-G.; Miyauchi, M. Efficient Visible Light Active $CaFe_2O_4/WO_3$ Based Composite Photocatalysts: Effect of Interfacial Modification. *Phys. Chem. C* **2009**, *113*, 17132–17137.
100. Jin, J.; Yu, J.; Guo, D.; Cui, C.; Ho, W. A Hierarchical Z-Scheme CdS–WO_3 Photocatalyst with Enhanced CO2 Reduction Activity. *Small* **2015**, *11*, 5262–5271.
101. Wang, J.; Yao, H.C.; Fan, Z.Y.; Zhang, L.; Li, Z.J. Indirect Z-Scheme BiOI/g-C3N4 Photocatalysts with Enhanced Photoreduction CO_2 Activity under Visible Light Irradiation. *ACS Appl. Mater. Interfaces* **2016**, *8*, 3765–3775.
102. Yang, H.G.; Sun, C.H.; Qiao, S.Z.; Zou, J.; Liu, G.; Smith, S.C.; Cheng, H.M.; Lu, G.Q. Anatase TiO_2 single crystals with a large percentage of reactive facets. *Nature* **2008**, *453*, 638–641.
103. Zhou, M.; Weng, Q.; Popov, Z.I.; Yang, Y.; Antipina, L.Y.; Sorokin, P.B.; Wang, X.; Bando, Y.; Golberg, D. Construction of Polarized Carbon–Nickel Catalytic Surfaces for Potent, Durable, and Economic Hydrogen Evolution Reactions. *ACS Nano* **2018**, *12*, 4148–4155.
104. Qu, S.; Chen, W.; Yu, J.; Chen, G.; Zhang, R.; Chu, S.; Huang, J.; Wang, X.; Li, C.; Ostrikov, K. Cross-linked trimetallic nanopetals for electrocatalytic water splitting. *Power Sources* **2018**, *390*, 224–233.
105. Zhang, C.; Zhou, Y.; Bao, J.; Sheng, X.; Fang, J.; Zhao, S.; Zhang, Y.; Chen, W. Hierarchical Honeycomb Br-, N-Codoped TiO_2 with Enhanced VisibleLight Photocatalytic H-2 Production. *ACS Appl. Mater. Interfaces* **2018**, *10*, 18796–18804.
106. Liu, Y.; Ding, S.; Shi, Y.; Liu, X.; Wu, Z.; Jiang, Q.; Zhou, T.; Liu, N.; Hu, J. Construction of CdS/CoOx core-shell nanorods for efficient photocatalytic H_2 *Appl. Catal. B* **2018**, *234*, 109–116.
107. Liang, S.; Han, B.; Liu, X.; Chen, W.; Peng, M.; Guan, G.; Deng, H.; Lin, Z. 3D spatially branched hierarchical Z-scheme CdS-Au nanoclusters-ZnO hybrids with boosted photocatalytic hydrogen evolution. *Alloys Compd.* **2018**, *754*, 105–113.
108. Li, J.; Peng, Y.; Qian, X.; Lin, J. Few-layer Co-doped MoS_2 nanosheets with rich active sites as an efficient cocatalyst for photocatalytic H_2 production over CdS. *Surf. Sci.* **2018**, *452*, 437–442.
109. Halasi, G.; Toth, A.; Bansagi, T.; Solymosi, F. Production of H_2 in the photocatalytic reactions of ethane on TiO_2-supported noble metals. *J. Hydrog. Energy* **2016**, *41*, 13485–13492.
110. Quan, Q.; Xie, S.; Weng, B.; Wang, Y.; Xu, Y.-J. Revealing the Double-Edged Sword Role of Graphene on Boosted Charge Transfer versus Active Site Control in TiO_2 Nanotube Arrays@RGO/MoS_2 *Small* **2018**, *14*, 1704531.
111. Fajrina, N.; Tahir, M. A critical review in strategies to improve photocatalytic water splitting towards hydrogen production. *J. Hydrog. Energy* **2019**, *44*, 540–577.
112. Xu, Y.; Xu, R. Nickel-based cocatalysts for photocatalytic hydrogen production. *Surf. Sci.* **2015**, *351*, 779–793.
113. Zhu, J.; Zäch, M. Nanostructured materials for photocatalytic hydrogen production. *Opin. Colloid Interface Sci.* **2009**, *14*, 260–269.
114. Acar, C.; Dincer, I.; Zamfirescu, C. A review on selected heterogeneous photocatalysts for hydrogen production. *J. Energy Res.* **2014**, *38*, 1903–1920.
115. Chiarello, G.L.; Aguirre, M.H.; Selli, E. Hydrogen production by photocatalytic steam reforming of methanol on noble metal-modified TiO_2. *Catal.* **2010**, *273*, 182–190.
116. Gupta, N.M. Factors affecting the efficiency of a water splitting photocatalyst: A perspective. *Sustain. Energy Rev.* **2017**, *71*, 585–601.
117. Houas, A.; Lachheb, H.; Ksibi, M.; Elaloui, E.; Guillard, C.; Herrmann, J.M. Photocatalytic degradation pathway of methylene blue in water. *Catal. B* 2001, 31, 145-157.
118. Lingampalli, S.R.; Ayyub, M.M.; Rao, C.N.R. Recent Progress in the Photocatalytic Reduction of Carbon Dioxide. *ACS Omega* **2017**, *2*, 2740–2748.
119. Xue, X.; Chen, R.; Yan, C.; Zhao, P.; Hu, Y.; Zhang, W.; Yang, S.; Zhong, J. Review on photocatalytic and electrocatalytic artificial nitrogen fixation for ammonia synthesis at mild conditions: Advances, challenges and perspectives. *Nano Res.* **2019**, *12*, 1229–1249.
120. Liu, B.; Aydil, E.S. Growth of Oriented Single-crystalline Rutile TiO_2 Nanorods on Transparent Conducting Substrates for Dye-sensitizedsolar Cells. *Am. Chem. Soc.* **2009**, *131*, 3985–3990.
121. Takeuchi, M.; Martra, G.; Coluccia, S.; Anpo, M. Investigations of the Structure of H2O Clusters Adsorbed on TiO_2 Surfaces by Near-Infrared Absorption Spectroscopy. *Phys. Chem. B* **2005**, *109*, 7387–7391.
122. Li, R.G.; Weng, Y.X.; Zhou, X.; Wang, X.L.; Mi, Y.; Chong, R.F.; Han, H.X.; Li, C. Achieving overall water splitting using titanium dioxide-based photocatalysts of different phases. *Energy Environ. Sci.* **2015**, *8*, 2377–2382.
123. Jitputti, J.; Suzuki, Y.; Yoshikawa, S. Synthesis of TiO_2 nanowires and their photocatalytic activity for hydrogen evolution. *Commun.* **2008**, *9*, 1265–1271.
124. Yang, Y.; Liu, G.; Irvine, J.T.S.; Cheng, H.-M. Enhanced Photocatalytic H-2 Production in Core-Shell Engineered Rutile TiO_2. *Mater.* **2016**, *28*, 5850–5856.

125. Li, L.; Yan, J.; Wang, T.; Zhao, Z.J.; Zhang, J.; Gong, J.; Guan, N. Sub-10nm rutile titanium dioxide nanoparticles for efficient visible-light-driven photocatalytic hydrogen production. *Commun.* **2015**, *6*, 5881.
126. Kavan, L.; Grätzel, M.; Gilbert, S.E.; Klemenz, C.; Scheel, H.J. Electrochemical and Photoelectrochemical Investigation of Single-Crystal Anatase. *Am. Chem. Soc.* **1996**, *118*, 6716–6723.
127. Kho, Y.K.; Iwase, A.; Teoh, W.Y.; Madler, L.; Amal, R. Photocatalytic H2 Evolution over TiO_2 The Synergistic Effect of Anatase and Rutile. *J. Phys. Chem. C* **2010**, *114*, 2821–2829.
128. Tian, J.; Leng, Y.; Zhao, Z.; Xia, Y.; Sang, Y.; Hao, P.; Zhan, J.; Li, M.; Liu, H. Carbon quantum dots/hydrogenated TiO_2 nanobelt heterostructures and their broad spectrum photocatalytic properties under UV, visible, and near-infrared irradiation. *Nano Energy* **2015**, *11*, 419–427.
129. Vequizo, J.J.M.; Matsunaga, H.; Ishiku, T.; Kamimura, S.; Ohno, T.; Yamakata, A. Trapping-Induced Enhancement of Photocatalytic Activity on Brookite TiO_2 Powders: Comparison with Anatase and Rutile TiO_2 *ACS Catal.* **2017**, *7*, 2644–2651.
130. Yu, J.; Low, J.; Xiao, W.; Zhou, P.; Jaroniec, M. Enhanced Photocatalytic CO_2-Reduction Activity of Anatase TiO_2 by Coexposed {001} and {101} Facets. *Am. Chem. Soc.* **2014**, *136*, 8839–8842.
131. Gao, C.; Wei, T.; Zhang, Y.; Song, X.; Huan, Y.; Liu, H.; Zhao, M.; Yu, J.; Chen, X. A Photoresponsive Rutile TiO_2 Heterojunction with Enhanced Electron–Hole Separation for High-Performance Hydrogen Evolution. *Mater.* **2019**, *13*, 1806596.
132. Yang, P.; Zhao, D.; Margolese, D.I.; Chmelka, B.F.; Stucky, G.D. Generalized syntheses of large-pore mesoporous metal oxides with semicrystalline frameworks. *Nature* **1998**, *396*, 152–155.
133. Ivanova, A.; Fattakhova-Rohlfing, D.; Kayaalp, B.E.; Rathousky, J.; Bein, T. Tailoring the Morphology of Mesoporous Titania Thin Films through Biotemplating with Nanocrystalline Cellulose. *Am. Chem. Soc.* **2014**, *136*, 5930–5937.
134. Crossland, E.J.W.; Noel, N.; Sivaram, V.; Leijtens, T.; Snaith, H.J. Mesoporous TiO_2 single crystals delivering enhanced mobility and optoelectronic device performance. *Nature* **2013**, *495*, 215.
135. Wei, L.; Wu, Z.; Wang, J.; Elzatahry, A.A.; Zhao, D. A Perspective on Mesoporous TiO_2 *Chem. Mater.* **2013**, *26*, 287–298.
136. Zhou, W.; Fu, H. ChemInform Abstract: Mesoporous TiO_2: Preparation, Doping, and as a Composite for Photocatalysis. *ChemCatChem* **2013**, *44*, 855.
137. Li, H.; Bian, Z.; Zhu, J.; Huo, Y.; Li, H.; Lu, Y. Mesoporous Au/TiO_2 Nanocomposites with Enhanced Photocatalytic Activity. *Am. Chem. Soc.* **2007**, *129*, 4538–4539.
138. Bach, U.; Lupo, D.; Comte, P.; Moser, J.E.; Weissortel, F.; Salbeck, J.; Spreitzer, H.; Gratzel, M. Solid-state dye-sensitized mesoporous TiO_2 solar cells with high photon-to-electron conversion efficiencies. Nature 1998, 395, 583-585.
139. Lee, J.; Orilall, M.; Warren, S.C.; Kamperman, M.; Disalvo, F.J.; Wiesner, U. Direct access to thermally stable and highly crystalline mesoporous transition-metal oxides with uniform pores.*Mater.* **2008**, *7*, 222–228.
140. Zhou, W.; Sun, F.; Pan, K.; Tian, G.; Jianga, B.; Ren, Z.; Tian, C.; Fu, H. Well-Ordered Large-Pore Mesoporous Anatase TiO_2 with Remarkably High Thermal Stability and Improved Crystallinity: Preparation, Characterization, and Photocatalytic Performance. *Funct. Mater.* **2011**, *21*, 1922–1930.
141. Zhou, W.; Li, W.; Wang, J.Q.; Qu, Y.; Yang, Y.; Xie, Y.; Zhang, K.; Wang, L.; Fu, H.; Zhao, D. Ordered Mesoporous Black TiO_2 as Highly Efficient Hydrogen Evolution Photocatalyst. *Am. Chem. Soc.* **2014**, *136*, 9280–9283.
142. Liu, P.; Yun, W.; Zhang, H.; An, T.; Yang, H.; Tang, Z.; Cai, W.; Zhao, H. Vapor-Phase Hydrothermal Transformation of HTiOF3 Intermediates into {001} Faceted Anatase Single-Crystalline Nanosheets. *Small* **2012**, *8*, 3664–3673.
143. Selcuk, S.; Selloni, A. Facet-dependent trapping and dynamics of excess electrons at anatase TiO_2 surfaces and aqueous interfaces. *Mater.* **2016**, *15*, 1107–1112.
144. Diebold, U. The Surface Science of Titanium Dioxide. *Rep.* **2003**, *48*, 53–229.
145. Yang, H.; Liu, G.; Qiao, S.; Jin, Y.; Smith, S.; Zou, J.; Cheng, H.-M.; Lu, M. Solvothermal Synthesis and Photoreactivity of Anatase TiO_2 Nanosheets With Dominant {001} Facets. *Am. Chem. Soc.* **2009**, *131*, 4078–4083.
146. Li, M.; Chen, Y.; Li, W.; Li, X.; Han, G. Ultrathin Anatase TiO_2 Nanosheets for High-Performance Photocatalytic Hydrogen Production. *Small* **2017**, *13*, 1604115.
147. Yang, J.; Wang, D.; Han, H.; Li, C. Roles of Cocatalysts in Photocatalysis and Photoelectrocatalysis. *Chem. Res.* **2013**, *46*, 1900–1909.
148. Mubeen, S.; Lee, J.; Singh, N.; Krämer, S.; Stucky, G.D.; Moskovits, M.J. An autonomous photosynthetic device in which all charge carriers derive from surface plasmons. *Nanotechnol.* **2013**, *8*, 247–251.
149. Zhang, Q.; Li, Z.; Wang, S.; Li, R.; Zhang, X.; Liang, Z.X.; Han, H.; Liao, S.; Li, C. The Effect of Redox Cocatalysts Location on Photocatalytic Overall Water Splitting over Cubic NaTaO3 Semiconductor Crystals Exposed with Equivalent Facets. *ACS Catal.* **2016**, *6*, 2182–2191.
150. Zhang, F.; Yamakata, A.; Maeda, K.; Moriya, Y.; Takata, T.; Kubota, J.; Teshima, K.; Oishi, S.; Domen, K. Cobalt-Modified Porous Single-Crystalline $LaTiO_2$ for Highly Efficient Water Oxidation under Visible Light. *Am. Chem. Soc.*

2012, *134*, 8348–8351.

151. Wu, J.; Jung, J.; Zhang, P.; Zhang, H.; Tang, J.; Le Guennic, B. Cis–trans isomerism modulates the magnetic relaxation of dysprosium single-molecule magnets. *Sci.* **2016**, *7*, 890–895.
152. Lu, J.; Elam, J.W.; Stair, P.C. Synthesis and Stabilization of Supported Metal Catalysts by Atomic Layer Deposition. *Chem. Res.* **2013**, *46*, 1806–1815.
153. Zhang, J.; Yu, Z.; Gao, Z.; Ge, H.; Zhao, S.; Chen, C.; Chen, S.; Tong, X.; Wang, M.; Zheng, Z.; et al. Porous TiO_2 Nanotubes with Spatially Separated Platinum and CoOx Cocatalysts Produced by Atomic Layer Deposition for Photocatalytic Hydrogen Production. *Chem. Int. Ed.* **2017**, *56*, 816–820.
154. Alenzi, N.; Liao, W.-S.; Cremer, P.S.; Sanchez-Torres, V.; Wood, T.K.; Ehlig-Economides, C.; Cheng, Z. Photoelectrochemical hydrogen production from water/methanol decomposition using Ag/TiO_2 nanocomposite thin films. *J. Energy Res.* **2010**, *35*, 11768–11775.
155. Mazheika, A.S.; Bredow, T.; Matulis, V.E.; Ivashkevich, O.A. Theoretical Study of Adsorption of Ag Clusters on the Anatase TiO_2(100) Surface. *Phys. Chem. C* **2011**, *115*, 17368–17377.
156. Zhou, J.; Takeuchi, M.; Ray, A.K.; Anpo, M.; Zhao, X.S. Enhancement of photocatalytic activity of P25 TiO_2 by vanadium-ion implantation under visible light irradiation. *Colloid Interface Sci.* **2007**, *311*, 497–501.
157. Seo, H.; Baker, L.R.; Hervier, A.; Kim, J.; Whitten, J.L.; Somorjai, G.A. Generation of Highly n-Type Titanium Oxide Using Plasma Fluorine Insertion. *Nano Lett.* **2011**, *11*, 751–756.
158. Xu, Y.; Zhang, C.; Zhang, L.; Zhang, X.; Yao, H.; Shi, J. Pd-catalyzed instant hydrogenation of TiO_2 with enhanced photocatalytic performance. *Energy Environ. Sci.* **2016**, *9*, 2410–2417.
159. Meng, Q.; Liu, B.; Liu, H.; Cai, Y.; Dong, L. Effects of S and Ta codoping on photocatalytic activity of rutile TiO_2. *Sol-Gel Sci. Technol.* 2018, 86, 631-639.
160. Lindgren, T.; Mwabora, J.M.; Avendaño, E.; Jonsson, J.; Hoel, A.; Granqvist, C.-G.; Lindquist, S.-E. Photoelectrochemical and Optical Properties of Nitrogen Doped Titanium Dioxide Films Prepared by Reactive DC Magnetron Sputtering. *Phys. Chem. B* **2003**, *107*, 5709–5716.
161. Diwald, O.; Thompson, T.L.; Zubkov, T.; Goralski, E.G.; Walck, S.D.; Yates, J.T. Photochemical activity of nitrogen-doped rutile TiO_2(111) in visible light. *Phys. Chem. B* **2004**, *108*, 6004–6008.
162. Sun, S.; Gao, P.; Yang, Y.; Yang, P.; Chen, Y.; Wang, Y. N-Doped TiO_2 Nanobelts with Coexposed (001) and (101) Facets and Their Highly Efficient Visible-Light-Driven Photocatalytic Hydrogen Production. *ACS Appl. Mater. Interfaces* **2016**, *8*, 18126–18131.
163. Umebayashi, T.; Yamaki, T.; Itoh, H.; Asai, K. Band Gap Narrowing of Titanium Dixode by Sulfur Doping. *Phys. Lett.* **2002**, *81*, 454–456.
164. Zhang, H.; Chen, G.; Bahnemann, D. Photoelectrocatalytic Materials for Environmental Applications. *Mater. Chem.* **2009**, *19*, 5089–5121.
165. Ouyang, J.; Chang, M.; Li, X.-J. CdS-sensitized ZnO nanorod arrays coated with TiO_2 layer for visible light photoelectrocatalysis. *Mater. Sci.* **2012**, *47*, 4187–4193.
166. Kim, J.; Kang, M. High photocatalytic hydrogen production over the band gap-tuned urchin-like Bi_2S_3-loaded TiO_2 composites system. *J. Hydrog. Energy* **2012**, *37*, 8249–8256.
167. Chai, B.; Peng, T.; Mao, J.; Li, K.; Zan, L. Graphitic carbon nitride (g-C3N4)-Pt-TiO_2 nanocomposite as an efficient photocatalyst for hydrogen production under visible light irradiation. *Chem. Chem. Phys.* **2012**, *14*, 16745–16752.
168. Xing, Z.; Li, Z.; Wu, X.; Wang, G.; Zhou, W. In-situ S-doped porous anatase TiO_2 nanopillars for high-efficient visible-light photocatalytic hydrogen evolution. *J. Hydrog. Energy* **2016**, *41*, 1535–1541.
169. Yang, Y.; Ye, K.; Cao, D.; Gao, P.; Qiu, M.; Liu, L.; Yang, P. Efficient Charge Separation from F– Selective Etching and Doping of Anatase-TiO_2{001} for Enhanced Photocatalytic Hydrogen Production. *ACS Appl. Mater. Interfaces* **2018**, *10*, 19633–19638.
170. Wang, X.; Chen, B.; Yan, D.; Zhao, X.; Wang, C.; Liu, E.; Zhao, N.; He, F. Distorted 1T-ReS2 Nanosheets Anchored on Porous TiO_2 Nanofibers for Highly Enhanced Photocatalytic Hydrogen Production. *ACS Appl. Mater. Interfaces* **2019**, *11*, 23144–23151.
171. Zhu, Y.; Li, J.; Dong, C.-L.; Ren, J.; Huang, Y.-C.; Zhao, D.; Cai, R.; Wei, D.; Yang, X.; Lv, C.; et al. Red phosphorus decorated and doped TiO_2 nanofibers for efficient photocatalytic hydrogen evolution from pure water. *Catal. B* **2019**, *255*, 117764.
172. Feng, W.; Hu, X.; Fan, J.; Liu, E.; Tao, S.; Kang, L.; Hou, W.; Zhu, C.; Liu, H. Photocatalytic Activity of Ag/TiO_2 Nanotube Arrays Enhanced by Surface Plasmon Resonance and Application in Hydrogen Evolution by Water Splitting. *Plasmonics* **2013**, *8*, 501–508.
173. Sun, T.; Fan, J.; Liu, E.; Liu, L.; Wang, Y.; Dai, H.; Yang, Y.; Hou, W.; Hu, X.; Jiang, Z. Fe and Ni co-doped TiO_2 nanoparticles prepared by alcohol-thermal method: Application in hydrogen evolution by water splitting under visible light irradiation. *Powder Technol.* **2012**, *228*, 210–218.

174. Kong, X.; Gao, Z.; Gong, Y.; Huang, H.; Wang, H.; Liu, P.; Yin, H.; Cui, Z.; Li, Z.; Liang, Y.; et al. Enhancement of photocatalytic H2 production by metal complex electrostatic adsorption on TiO_2 (B) nanosheets. *Mater. Chem. A* **2019**, *7*, 3797–3804.
175. Huang, J.; Li, G.; Zhou, Z.; Jiang, Y.; Hu, Q.; Xue, C.; Guo, W. Efficient photocatalytic hydrogen production over Rh and Nb codoped TiO_2 *Chem. Eng. J.* **2018**, *337*, 282–289.
176. Li, Y.; Ding, L.; Liang, Z.; Xue, Y.; Cui, H.; Tian, J. Synergetic effect of defects rich MoS2 and Ti3C2 MXene as cocatalysts for enhanced photocatalytic H_2 production activity of TiO_2. *Eng. J.* **2020**, *383*, 123178.
177. Chang, A.; Peng, W.-S.; Tsai, I.T.; Chiang, L.-F.; Yang, C.-M. Efficient hydrogen production by selective alcohol photoreforming on plasmonic photocatalyst comprising sandwiched Au nanodisks and TiO_2. *Catal. B* **2019**, *255*, 117773.
178. Han, X.; An, L.; Hu, Y.; Li, Y.; Hou, C.; Wang, H.; Zhang, Q. Ti_3C_2 MXene-derived carbon-doped TiO_2 coupled with g-C3N4 as the visible-light photocatalysts for photocatalytic H2 generation. *Catal. B* **2020**, *265*, 118539.
179. Tang, W.Z.; Huren, A. UV/TiO_2 photocatalytic oxidation of commercial dyes in aqueous solutions. *Chemosphere* **1995**, *31*, 4157–4170.
180. Pirkanniemi, K.; Sillanpää, M. Heterogeneous water phase catalysis as an environmental application: A review. *Chemosphere* **2002**, *48*, 1047–1060.
181. Jitianu, A.; Cacciaguerra, T.; Benoit, R.; Delpeux, S.; Béguin, F.; Bonnamy, S. Synthesis and characterization of carbon nanotubes–TiO_2 *Carbon* **2004**, *42*, 1147–1151.
182. Gao, B.; Chen, G.Z.; Li Puma, G. Carbon nanotubes/titanium dioxide (CNTs/TiO_2) nanocomposites prepared by conventional and novel surfactant wrapping sol–gel methods exhibiting enhanced photocatalytic activity. *Catal. B* **2009**, *89*, 503–509.
183. Woan, K.; Pyrgiotakis, G.; Sigmund, W. Photocatalytic Carbon-Nanotube–TiO_2 *Adv.Mater.* **2009**, *21*, 2233–2239.
184. Natarajan, T.S.; Lee, J.Y.; Bajaj, H.C.; Jo, W.-K.; Tayade, R.J. Synthesis of multiwall carbon nanotubes/TiO_2 nanotube composites with enhanced photocatalytic decomposition efficiency. *Today* **2017**, *282*, 13–23.
185. Azzam, E.M.S.; Fathy, N.A.; El-Khouly, S.M.; Sami, R.M. Enhancement the photocatalytic degradation of methylene blue dye using fabricated CNTs/TiO_2/AgNPs/Surfactant nanocomposites. *Water Process. Eng.* **2019**, *28*, 311–321.
186. Hirakawa, T.; Kamat, P.V. Charge Separation and Catalytic Activity of Ag@TiO_2 Core Shell Composite Clusters under UV–Irradiation. *Am. Chem. Soc.* **2005**, *127*, 3928–3934.
187. Subramanian, V.; Wolf, E.E.; Kamat, P.V. Catalysis with TiO_2/Gold Nanocomposites. Effect of Metal Particle Size on the Fermi Level Equilibration. *Am. Chem. Soc.* **2004**, *126*, 4943–4950.
188. Yoskamtorn, T.; Yamazoe, S.; Takahata, R.; Nishigaki, J.I.; Thivasasith, A.; Limtrakul, J.; Tsukuda, T. Thiolate-Mediated Selectivity Control in Aerobic Alcohol Oxidation by Porous Carbon-Supported Au Clusters. *ACS Catal.* **2014**, *4*, 3696–3700.
189. Zhu, H.; Goswami, N.; Yao, Q.; Chen, T.; Liu, Y.; Xu, Q.; Chen, D.; Lu, J.; Xie, J. Cyclodextrin-gold nanocluster decorated TiO_2 enhances photocatalytic decomposition of organic pollutants. *Mater. Chem. A* **2018**, *6*, 1102.
190. Qiao, B.; Wang, A.; Yang, X.; Allard, L.F.; Jiang, Z.; Cui, Y.; Liu, J.; Li, J.; Zhang, T. Single-atom catalysis of CO oxidation using Pt1/FeOx. *Chem.* **2011**, *3*, 634–641.
191. Ding, K.; Gulec, A.; Johnson, A.M.; Schweitzer, N.M.; Stucky, G.D.; Marks, L.D.; Stair, P.C. Identification of active sites in CO oxidation and water-gas shift over supported Pt catalysts. *Science* **2015**, *350*, 189–192.
192. Yang, M.; Li, S.; Wang, Y.; Herron, J.A.; Xu, Y.; Allard, L.F.; Lee, S.; Huang, J.; Mavrikakis, M.; Flytzani-Stephanopoulos, M. Catalytically active Au-O(OH)x- species stabilized by alkali ions on zeolites and mesoporous oxides. *Science* **2014**, *346*, 1498–1501.
193. Wang, Y.; Zhao, X.; Cao, D.; Wang, Y.; Zhu, Y. Peroxymonosulfate enhanced visible light photocatalytic degradation bisphenol A by single-atom dispersed Ag mesoporous g-C_3N_4 *Appl. Catal. B* **2017**, *211*, 79–88.
194. Xu, T.; Zhao, H.; Zheng, H.; Zhang, P. Atomically Pt implanted nanoporous TiO_2 film for photocatalytic degradation of trace organic pollutants in water. *Eng. J.* **2020**, *385*, 123832.
195. Gang, L.; Lu, L.; Fan, H.; Ma, J.; Li, Y.; Yong, W.; Zhao, X.S. Effect of the agglomeration of TiO_2 nanoparticles on their photocatalytic performance in the aqueous phase. *Colloid Interface Sci.* **2010**, *348*, 342–347.
196. French, R.A.; Jacobson, A.R.; Kim, B.; Isley, S.L.; Penn, R.L.; Baveye, P.C. Influence of Ionic Strength, Ph, and Cation Valence on Aggregation Kinetics of Titanium Dioxide Nanoparticles. *Sci. Technol.* **2009**, *43*, 1354–1359.
197. Zhe, D.; Hu, X.; Lu, G.Q.; Yue, P.L.; Greenfield, P.F. Novel Silica Gel Supported TiO_2 Photocatalyst Synthesized by CVD Method. *Langmuir* **2000**, *16*, 6216–6222.
198. Iwasaki, M.; Miyamoto, Y.; Ito, S.; Furuzono, T.; Park, W.K. Fabrication of platy apatite nanocrystals loaded with TiO_2 nanoparticles by two-step emulsion method and their photocatalytic activity. *Colloid Interface Sci.* **2008**, *326*, 537–540.
199. Li, Y.; Zhao, H.; Yang, M. TiO_2 nanoparticles supported on PMMA nanofibers for photocatalytic degradation of methyl orange. *Colloid Interface Sci.* **2017**, *508*, 500–507.

200. Alam, U.; Fleisch, M.; Kretschmer, I.; Bahnemann, D.; Muneer, M. One-step hydrothermal synthesis of Bi-TiO_2 nanotube/graphene composites: An efficient photocatalyst for spectacular degradation of organic pollutants under visible light irradiation. *Catal. B* **2017**, *218*, 758–769.
201. Wang, W.K.; Chen, J.J.; Gao, M.; Huang, Y.X.; Zhang, X.; Yu, H.Q. Photocatalytic Degradation of Atrazine by Boron-Doped TiO_2 with a Tunable Rutile/Anatase Ratio. *Catal. B* **2016**, *195*, 203–215.
202. Xing, H.; Wen, W.; Wu, J.-M. Enhanced UV photoactivity of Ti^{3+} self-doped anatase TiO_2 single crystals hydrothermally synthesized using Ti-H2O2-HF reactants. *Photochem. Photobiol. A* **2019**, *382*, 111958.
203. Nair, S.B.; K, A.j.; Menon, S.S.; Rahman, H.; Joseph, J.A.; Shaji, S.; Philip, R.R. Influence of electrochemical reduction of selfdoping on the low temperature crystallization and photocatalytic activities of TiO_2 *Semicond. Sci. Technol.* **2019**, *34*, 095023.
204. Liu, C.; Dong, S.; Chen, Y. Enhancement of visible-light-driven photocatalytic activity of carbon plane/g-C_3N_4/TiO_2 nanocomposite by improving heterojunction contact. *Eng. J.* **2019**, *371*, 706–718.
205. Yao, P.; Liu, H.; Wang, D.; Chen, J.; Li, G.; An, T. Enhanced visible-light photocatalytic activity to volatile organic compounds degradation and deactivation resistance mechanism of titania confined inside a metal-organic framework. *Colloid Interface Sci.* **2018**, *522*, 174–182.
206. Sheng, H.; Chen, D.; Li, N.; Xu, Q.; Li, H.; He, J.; Lu, J. Urchin-Inspired TiO_2@MIL-101 Double-Shell Hollow Particles: Adsorption and Highly Efficient Photocatalytic Degradation of Hydrogen Sulfide. *Mater.* **2017**, *29*, 5612–5616.
207. Sung-Suh, H.M.; Choi, J.R.; Hah, H.J.; Koo, S.M.; Bae, Y.C. Comparison of Ag deposition effects on the photocatalytic activity of nanoparticulate TiO_2 under visible and UV light irradiation. *Photochem. Photobiol. A* **2004**, *163*, 37–44.
208. Paramasivam, I.; Macak, J.M.; Schmuki, P. Photocatalytic activity of TiO_2 nanotube layers loaded with Ag and Au nanoparticles. *Commun.* **2008**, *10*, 71–75.
209. Yang, X.; Xu, L.; Yu, X.; Guo, Y. One-step preparation of silver and indium oxide co-doped TiO_2 photocatalyst for the degradation of rhodamine B. *Commun.* **2008**, *9*, 1224–1229.
210. Kowalska, E.; Remita, H.; Colbeau-Justin, C.; Hupka, J.; Belloni, J. Modification of Titanium Dioxide with Platinum Ions and Clusters: Application in Photocatalysis. *Phys. Chem. C* **2008**, *112*, 1124–1131.
211. Zhu, J.; Chen, F.; Zhang, J.; Chen, H.; Anpo, M. Fe^{3+}-TiO_2 photocatalysts prepared by combining sol–gel method with hydrothermal treatment and their characterization. *Photochem. Photobiol. A* **2006**, *180*, 196–204.
212. Li, H.; Duan, X.; Liu, G.; Li, L. Synthesis and characterization of copper ions surface-doped titanium dioxide nanotubes. *Res. Bull.* **2008**, *43*, 1971–1981.
213. Chen, C.; Wang, Z.; Ruan, S.; Zou, B.; Zhao, M.; Wu, F. Photocatalytic degradation of C.I. Acid Orange 52 in the presence of Zn-doped TiO_2 prepared by a stearic acid gel method. *Dyes Pigment.* **2008**, *77*, 204–209.
214. Zhang, S.; Chen, Y.; Yu, Y.; Wu, H.; Wang, S.; Zhu, B.; Huang, W.; Wu, S. Synthesis, characterization of Cr-doped TiO_2 nanotubes with high photocatalytic activity. *Nanopart. Res.* **2008**, *10*, 871–875.
215. Geng, J.; Jiang, Z.; Wang, Y.; Yang, D. Carbon-modified TiO_2 nanotubes with enhanced photocatalytic activity synthesized by a facile wet chemistry method. *Mater.* **2008**, *59*, 352–355.
216. Zhao, L.; Jiang, Q.; Lian, J. Visible-light photocatalytic activity of nitrogen-doped TiO_2 thin film prepared by pulsed laser deposition. *Surf. Sci.* **2008**, *254*, 4620–4625.
217. Liu, G.; Zhao, Y.; Sun, C.; Li, F.; Lu, G.Q.; Cheng, H.-M. Synergistic Effects of B/N Doping on the Visible-Light Photocatalytic Activity of Mesoporous TiO_2. *Chem. Int. Ed.* **2008**, *47*, 4516–4520.
218. Wei, F.; Ni, L.; Cui, P. Preparation and characterization of N–S-codoped TiO_2 photocatalyst and its photocatalytic activity. *Hazard. Mater.* **2008**, *156*, 135–140.
219. Suárez-Parra, R.; Hernández-Pérez, I.; Rincón, M.E.; López-Ayala, S.; Roldán-Ahumada, M.C. Visible light-induced degradation of blue textile azo dye on TiO_2/CdO–ZnO coupled nanoporous films. *Energy Mater. Sol. Cells* **2003**, *76*, 189–199.
220. Ibhadon, A.O.; Greenway, G.M.; Yue, Y. Photocatalytic activity of surface modified TiO_2/RuO_2/SiO_2 nanoparticles for azo-dye degradation. *Commun.* **2008**, *9*, 153–157.
221. Ge, L.; Xu, M.; Fang, H. Photo-catalytic degradation of methyl orange and formaldehyde by Ag/InVO4–TiO_2 thin films under visible-light irradiation. *Mol. Catal. A Chem.* **2006**, *258*, 68–76.
222. Inoue, T.; Fujishima, A.; Konishi, S.; Honda, K. Photoelectrocatalytic reduction of carbon dioxide in aqueous suspensions of semiconductor powers. *Nature* **1979**, *277*, 637–638.
223. Meng, A.; Zhang, L.; Cheng, B.; Yu, J. Dual Cocatalysts in TiO 2 Photocatalysis. *Mate.* **2019**, *31*, 1807660.
224. Liu, Q.; Zhou, Y.; Kou, J.; Chen, X.; Tian, Z.; Gao, J.; Yan, S.; Zou, Z. High-Yield Synthesis of Ultralong and Ultrathin Zn_2GeO_4 Nanoribbons toward Improved Photocatalytic Reduction of CO_2 into Renewable Hydrocarbon Fuel. *Am. Chem. Soc.* **2010**, *132*, 14385–14387.
225. Li, D.; Kassymova, M.; Cai, X.; Zang, S.-Q.; Jiang, H.-L. Photocatalytic CO_2 reduction over metal-organic framework-based materials. *Chem. Rev.* 2020, 412.

226. Manzanares, M.; Gallego, C.F.; Ossó, J.O.; Vega, L.F.; Andreu, T.; Morante, J.R. Engineering the TiO_2 outermost layers using magnesium for carbon dioxide photoreduction. *Catal. B* **2014**, *150–151*, 57–62.
227. Tseng, I.H.; Wu, J.C.-S. Chemical states of metal-loaded titania in the photoreduction of CO2. *Today* **2004**, *97*, 113–119.
228. Xie, S.; Wang, Y.; Zhang, Q.; Fan, W.; Deng, W.; Wang, Y. Photocatalytic reduction of CO_2 with H_2O: Significant enhancement of the activity of Pt–TiO_2 in CH4 formation by addition of MgO. *Commun.* **2013**, *49*, 2451–2453.
229. Li, H.; Li, C.; Han, L.; Li, C.; Zhang, S.-J. Photocatalytic reduction of CO_2 with H_2O on CuO/TiO_2 *Energy Sources Part A* **2016**, *38*, 420–426.
230. Bessekhouad, Y.; Robert, D.; Weber, J.V. Bi_2S_3/TiO_2 and CdS/TiO_2 heterojunctions as an available configuration for photocatalytic degradation of organic pollutant. *Photochem. Photobiol. A* **2004**, *163*, 569–580.
231. McTiernan, C.D.; Pitre, S.P.; Ismaili, H.; Scaiano, J.C. Heterogeneous Light-Mediated Reductive Dehalogenations and Cyclizations Utilizing Platinum Nanoparticles on Titania (PtNP@TiO_2). *Synth. Catal.* 2014, 356, 2819-2824.
232. Wang, K.; Zhang, Y.; Liu, L.; Lu, N.; Zhang, Z. BiOBr nanosheets-decorated TiO_2 nanofibers as hierarchical p–n heterojunctions photocatalysts for pollutant degradation. *Mater. Sci.* **2019**, *54*, 8426–8435.
233. Meng, A.; Zhang, L.; Cheng, B.; Yu, J. TiO_2–MnOx–Pt Hybrid Multiheterojunction Film Photocatalyst with Enhanced Photocatalytic CO_2-Reduction Activity. *ACS Appl. Mater. Interfaces* **2019**, *11*, 5581–5589.
234. Luo, L.; Maggard, P.A. Effect of Ligand Coordination on the Structures and Visible-Light Photocatalytic Activity of Manganese Vanadate Hybrids. *Growth Des.* **2013**, *13*, 5282–5288.
235. Mu, X.; Jiang, J.; Chao, F.; Lou, Y.; Chen, J. Ligand modification of UiO-66 with an unusual visible light photocatalytic behavior for RhB degradation. *Dalton Trans.* **2018**, *47*, 1895–1902.
236. Liu, L.; Zhao, C.; Li, Y. Spontaneous Dissociation of CO_2 to CO on Defective Surface of Cu(I)/TiO_2–x Nanoparticles at Room Temperature. *Phys. Chem. C* **2012**, *116*, 7904–7912.
237. Jeong, S.; Kim, G.-M.; Kang, G.-S.; Kim, C.; Lee, H.; Kim, W.-J.; Lee, Y.K.; Lee, S.; Kim, H.; Lim, H.K.; et al. Selectivity Modulated by Surface Ligands on Cu_2O/TiO_2 Catalysts for Gas-Phase Photocatalytic Reduction of Carbon Dioxide. *Phys. Chem. C* **2019**, *123*, 29184–29191.
238. Pham, T.D.; Lee, B.K. Novel capture and photocatalytic conversion of CO_2 into solar fuels by metals co-doped TiO_2 deposited on PU under visible light. *Catal. A* **2017**, *529*, 40–48.
239. Dong, X.; Li, F.; Zhao, N.; Xiao, F.; Wang, J.; Tan, Y. CO2 hydrogenation to methanol over Cu/ZnO/ZrO_2 catalysts prepared by precipitation-reduction method. *Catal. B* **2016**, *191*, 8–17.
240. Singh, S.; Verma, N. Graphitic carbon micronanofibers asymmetrically dispersed with alumina-nickel nanoparticles: A novel electrode for mediatorless microbial fuel cells. *J. Hydrog. Energy* **2015**, *40*, 5928–5938.
241. Modi, A.; Singh, S.; Verma, N. In situ nitrogen-doping of nickel nanoparticle-dispersed carbon nanofiber-based electrodes: Its positive effects on the performance of a microbial fuel cell. *Acta* **2016**, *190*, 620–627.
242. Sharma, A.; Lee, B.-K. Photocatalytic reduction of carbon dioxide to methanol using nickel-loaded TiO_2 supported on activated carbon fiber. *Today* **2017**, *298*, 158–167.
243. Hsu, H.-C.; Shown, I.; Wei, H.-Y.; Chang, Y.-C.; Du, H.-Y.; Lin, Y.-G.; Tseng, C.-A.; Wang, C.-H.; Chen, L.-C.; Lin, Y.-C.; et al. Graphene oxide as a promising photocatalyst for CO2 to methanol conversion. *Nanoscale* **2012**, *5*, 262–268.
244. Kumar, P.; Mungse, H.; Khatri, O.; Jain, S. Nitrogen-doped graphene-supported copper complex: A novel photocatalyst for CO_2 reduction under visible light irradiation. *RSC Adv.* **2015**, *5*, 54929–54935.
245. Kumar, P.; Joshi, C.; Labhsetwar, N.; Boukherroub, R.; Jain, S. A novel Ru/TiO_2 hybrid nanocomposite catalyzed photoreduction of CO_2 to methanol under visible light. *Nanoscale* **2015**, *7*, 15258–15267.
246. Cheng, J.; Zhang, M.; Wu, G.; Wang, X.; Zhou, J.; Cen, K. Photoelectrocatalytic Reduction of CO_2 into Chemicals Using Pt-Modified Reduced Graphene Oxide Combined with Pt-Modified TiO_2 *Environ. Sci. Technol.* **2014**, *48*, 7076–7084.
247. Rambabu, Y.; Kumar, U.; Singhal, N.; Kaushal, M.; Jaiswal, M.; Jain, S.L.; Roy, S.C. Photocatalytic reduction of carbon dioxide using graphene oxide wrapped TiO_2 *Appl. Surf. Sci.* **2019**, *485*, 48–55.
248. Xue, L.M.; Zhang, F.H.; Fan, H.J.; Bai, X.F. Preparation of C Doped TiO_2 Photocatalysts and their Photocatalytic Reduction of Carbon Dioxide. *Mater. Res.* **2011**, *183-185*, 1842-1846.
249. Michalkiewicz, B.; Majewska, J.; Kądziołka, G.; Bubacz, K.; Mozia, S.; Morawski, A.W. Reduction of CO_2 by adsorption and reaction on surface of TiO_2-nitrogen modified photocatalyst. *CO_2 Util.* **2014**, *5*, 47–52.
250. Phongamwong, T.; Chareonpanich, M.; Limtrakul, J. Role of chlorophyll in Spirulina on photocatalytic activity of CO_2 reduction under visible light over modified N-doped TiO_2 *Appl. Catal. B* **2015**, *168–169*, 114–124.
251. Ola, O.; Maroto-Valer, M.M. Transition metal oxide based TiO_2 nanoparticles for visible light induced CO2 photoreduction. *Catal. A* **2015**, *502*, 114–121.
252. Tahir, M.; Amin, N.S. Indium-doped TiO_2 nanoparticles for photocatalytic CO_2 reduction with H2O vapors to CH4. *Catal. B* **2015**, *162*, 98–109.

253. Kong, D.; Tan, J.Z.Y.; Yang, F.; Zeng, J.; Zhang, X. Electrodeposited Ag nanoparticles on TiO_2 nanorods for enhanced UV visible light photoreduction CO_2 to CH_4. *Surf. Sci.* **2013**, *277*, 105–110.
254. Mao, J.; Ye, L.; Li, K.; Zhang, X.; Liu, J.; Peng, T.; Zan, L. Pt-loading reverses the photocatalytic activity order of anatase TiO_2 {001} and {010} facets for photoreduction of CO_2 to CH_4. *Catal. B* **2014**, *144*, 855–862.
255. Tahir, B.; Tahir, M.; Amin, N.A.S. Photocatalytic CO_2 conversion over Au/TiO_2 nanostructures for dynamic production of clean fuels in a monolith photoreactor. *Clean Technol. Environ. Policy* **2016**, *18*, 2147–2160.
256. Beigi, A.A.; Fatemi, S.; Salehi, Z. Synthesis of nanocomposite CdS/TiO_2 and investigation of its photocatalytic activity for CO2 reduction to CO and CH4 under visible light irradiation. *CO_2 Util.* **2014**, *7*, 23–29.
257. Mele, G.; Annese, C.; De Riccardis, A.; Fusco, C.; Palmisano, L.; Vasapollo, G.; D'Accolti, L. Turning lipophilic phthalocyanines/TiO_2 composites into efficient photocatalysts for the conversion of CO_2 into formic acid under UV–vis light irradiation. *Catal. A* **2014**, *481*, 169–172.
258. Erisman, J.W.; Sutton, M.; Galloway, J.; Klimont, Z.; Winiwarter, W. How a century of ammonia synthesis changed the world. *Geosci.* **2008**, *1*, 636–639.
259. Licht, S.; Cui, B.; Wang, B.; Li, F.-F.; Lau, J.; Liu, S. ChemInform Abstract: Ammonia Synthesis by N2 and Steam Electrolysis in Molten Hydroxide Suspensions of Nanoscale Fe_2O_3. *ChemInform* **2014**, *45*, 45.
260. Li, J.; Li, H.; Zhan, G.; Zhang, L. Solar Water Splitting and Nitrogen Fixation with Layered Bismuth Oxyhalides. *Chem. Res.* **2017**, *50*, 112–121.
261. Schrauzer, G.N.; Guth, T.D. Photolysis of Water and Photoreduction of Nitrogen on Titanium Dioxide. *Am. Chem. Soc.* **1977**, *99*, 7189–7193.
262. Khader, M.M.; Lichtin, N.N.; Vurens, G.H.; Salmeron, M.; Somorjai, G.A. Photoassisted catalytic dissociation of water and reduction of nitrogen to ammonia on partially reduced ferric oxide. *Langmuir* **1987**, *3*, 303–304.
263. Xu, F.; Xu, C.; Wu, D.; Gao, Z.; Ma, X.; Jiang, K. Bi_2S_3/BiOBr hybrid structure prepared via anion exchange for enhanced photocatalytic nitrogen fixation performance. *Lett.* 2019, 253, 183-186.
264. Zhao, W.; Zhang, J.; Zhu, X.; Zhang, M.; Tang, J.; Tan, M.; Wang, Y. Enhanced nitrogen photofixation on Fe-doped TiO_2 with highly exposed (101) facets in the presence of ethanol as scavenger. *Catal. B* **2014**, *144*, 468–477.
265. Chen, D.; Jiang, Z.; Geng, J.; Wang, Q.; Yang, D. Carbon and Nitrogen Co-doped TiO_2 with Enhanced Visible-Light Photocatalytic Activity. *Eng. Chem. Res.* **2007**, *46*, 2741–2746.
266. Liu, Q.; Ai, L.; Jing, J. MXene-derived TiO_2@C/g-C_3N_4 heterojunctions for highly efficient nitrogen photofixation. *Mater. Chem. A* **2018**, *6*, 4102–4110.
267. Li, H.; Mao, C.; Shang, H.; Yang, Z.; Ai, Z.; Zhang, L. New Opportunities Opened by Nanosheets photocatalysts for Efficient N2 fixation. *Nanoscale* **2018**, *10*, 15429.
268. Zhao, Y.; Zhao, Y.; Waterhouse, G.I.N.; Zheng, L.; Cao, X.; Teng, F.; Wu, L.Z.; Tung, C.H.; O'Hare, D.; Zhang, T. Layered-Double-Hydroxide Nanosheets as Efficient Visible-Light-Driven Photocatalysts for Dinitrogen Fixation. *Mater.* **2017**, *29*, 1703828.
269. Zhao, Y.; Zhao, Y.; Shi, R.; Wang, B.; Waterhouse, G.I.N.; Wu, L.-Z.; Tung, C.-H.; Zhang, T. Tuning Oxygen Vacancies in Ultrathin TiO_2 Nanosheets to Boost Photocatalytic Nitrogen Fixation up to 700 nm. *Mater.* **2019**, *31*, 1806482.
270. Asbury, J.B.; Wang, Y.Q.; Hao, E.; Ghosh, H.N.; Lian, T. Evidences of hot excited state electron injection from sensitizer molecules to TiO_2 nanocrystalline thin films. *Chem. Intermed.* **2001**, *27*, 393–406.
271. Ji, P.; Takeuchi, M.; Cuong, T.M.; Zhang, J.; Matsuoka, M.; Anpo, M. Recent advances in visible light-responsive titanium oxide-based photocatalysts. *Chem. Intermed.* **2010**, *36*, 327–347.
272. Yang, Y.; Zhong, H.; Tian, C. Photocatalytic mechanisms of modified titania under visible light. *Chem. Intermed.* **2011**, *37*, 91–102.
273. Zhao, R.; Shen, D.; Xu, M.; Feng, D.; Li, W.; Zheng, G.; Che, R.; Elzatahry, A.A.; Zhao, D. Ordered Macro-/Mesoporous Anatase Films with High Thermal Stability and Crystallinity for Photoelectrocatalytic Water-Splitting %J Advanced Energy Materials. *Energy Mater.* **2014**, *4*, 1301725.
274. Wu, S.; Tan, X.; Liu, K.; Liu, Y.; Wang, L.; Zhang, J. TiO_2 (B) nanotubes with ultrathin shell for highly efficient photocatalytic fixation of nitrogen. *Today* **2019**, *335*, 214–220.
275. Li, H.; Shang, J.; Ai, Z.; Zhang, L. Efficient Visible Light Nitrogen Fixation with BiOBr Nanosheets of Oxygen Vacancies on the Exposed {001} Facets. *Am. Chem. Soc.* **2015**, *137*, 6393–6399.
276. Hirakawa, H.; Hashimoto, M.; Shiraishi, Y.; Hirai, T. Photocatalytic Conversion of Nitrogen to Ammonia with Water on Surface Oxygen Vacancies of Titanium Dioxide. *Am. Chem. Soc.* **2017**, *139*, 10929–10936.
277. Kong, M.; Li, Y.; Chen, X.; Tian, T.; Zhao, X. Tuning the Relative Concentration Ratio of Bulk Defects to Surface Defects in TiO_2 Nanocrystals Leads to High Photocatalytic Efficiency. *Am. Chem. Soc.* **2011**, *133*, 16414–16417.
278. Wang, J.; Lin, W.; Ran, Y.; Cui, J.; Wang, L.; Yu, X.; Zhang, Y. Nanotubular TiO_2 with Remedied Defects for Photocatalytic Nitrogen Fixation. *Phys. Chem. C* **2020**, *124*, 1253–1259.
279. Ileperuma, O.A.; Tennakone, K.; Dissanayake, W. Photocatalytic behaviour of metal doped titanium dioxide: Studies on the Photochemical Synthesis of Ammonia on Mg/TiO_2 Catalyst Systems. *Catal.* **1990**, *62*, L1–L5.

280. Palmisano, L.; Augugliaro, V.; Sclafani, A.; Schiavello, M. Activity of chromium-ion-doped titania for the dinitrogen photoreduction to ammonia and for the phenol photodegradation. *Phys. Chem.* **1988**, *92*, 6710–6713.
281. Ileperuma, O.A.; Thaminimulla, C.T.K.; Kiridena, W.C.B. Photoreduction of N_2 to NH_3 and H2O to H2 on metal doped TiO_2 catalysts (M = Ce, V). *Energy Mater. Sol. Cells* **1993**, *28*, 335–343.
282. Liu, S.; Wang, Y.; Wang, S.; You, M.; Hong, S.; Wu, T.-S.; Soo, Y.-L.; Zhao, Z.; Jiang, G.; Jieshan, Q.; et al. Photocatalytic Fixation of Nitrogen to Ammonia by Single Ru Atom Decorated TiO_2 *ACS Sustain. Chem. Eng.* **2019**, *7*, 6813–6820.
283. Chang, S.; Xu, X. Au nanocrystals decorated TiO_2 nanotubes for photocatalytic nitrogen fixation into ammonia. *Chem. Front.* **2020**, *7*, 620–624.
284. Hao, C.; Liao, Y.; Wu, Y.; An, Y.; Lin, J.; Gu, Z.; Jiang, M.; Hu, S.; Wang, X. RuO_2-loaded TiO_2–MXene as a high performance photocatalyst for nitrogen fixation. *Phys. Chem. Solids* **2020**, *136*, 109141.